Dissertation zur Erlangung des Doktorgrades

der Fakultät für Chemie und Pharmazie

der Ludwig-Maximilians-Universität München

Molecular Mechanisms of

Phase Separation during RISC loading in

Drosophila melanogaster

Selina Mußgnug

aus

Pforzheim, Deutschland

2023

Summary

RNA interference is a post-transcriptional gene-regulatory pathway that is guided by small RNAs. In *Drosophila melanogaster* RNA silencing is directed by miRNAs (gene regulation) and siRNAs (defense against viruses and endogenous transposons) derived from longer double-stranded precursors by nucleolytic processing through Dicer-like enzymes. miRNAs originate from genomic loci that are located in intergenic regions or protein-coding genes transcribed by RNA Pol II. Dcr-1 works in complex with dsRNA-binding protein Loqs-PB to process the precursor into mature miRNA in the cytoplasm. The mature miRNA is loaded into the effector endonuclease Ago1. GW182, an RNA-binding protein, localizes Ago1 to P-bodies where mRNA targets are decayed or stored. Long double stranded siRNA precursors can be introduced into a cell from exogenous (RNA virus) or endogenous sources (transposons). The dsRNA is processed by a complex of Dcr-2 and dsRNA binding protein R2D2 or its paralog Loqs-PD and the resulting siRNA is loaded into Ago2 (RNA induced silencing complex). The detection of fully complementary sequences within target RNAs by the RNA induced silencing complex results in Ago2-mediated cleavage of the RNA target. Previous studies showed that R2D2 co-condensates with Dcr-2 in membrane-less organelles called D2-bodies that are formed through liquid-liquid phases separation. Like many proteins that undergo phase separation, Loqs-PD and Ago2 both have a low complexity intrinsically disordered region in the N-terminus that is predicted to be prion-like. Furthermore, Loqs-PD has two double-stranded RNA binding domains that are connected by an unstructured linker. These dsRNA binding domains are suspected to be stickers and the linker to be a spacer. Stickers in folded protein domains are surfaces patches or motifs that emerge from the formation of specific structures. Non-sticker regions and disordered loop regions can be considered as spacers. RNA is an ideal scaffold for condensate formation as it provides binding sites to proteins through its long length, flexibility and multivalency. To investigate whether Loqs-PD forms condensates in the cytoplasm of *Drosophila cells*, GFP-Loqs-PD fusion constructs were cloned, transiently transfected and the localization of the protein was examined via live cell imaging. Loqs-PD forms condensates in the cytoplasm that exhibit a partially liquid-like nature and their formation is reversible as shown by FRAP assay and 1,6-hexanediol treatment. The binding capability of dsRBD2 is crucial for condensate formation since point mutations in the dsRBD2 that prevent binding of dsRNA lead to a reduced number of condensates in cells. Moreover, immunostaining of Dcr-2 and Loqs-PD revealed their co-localization to the same cytoplasmic condensates resembling the D2 bodies formed by Dcr-2/R2D2. The visualization of the localization of Ago2 and its role in the context of condensate

formation are still to be investigated since many attempts to generate fusions with fluorescent proteins were not successful during this study. One major problem was a protease sensitive site in the N-terminus of Ago2 which made it difficult to generate a functional N-terminal fusion protein to examine the localization of Ago2 in cells.

Table of Contents

Parts of this thesis are intended to be part of a publication.

1 Introduction

1.1 RNA interference

RNA interference (RNAi) is a small RNA-mediated, conserved regulatory mechanism involved in processes like gene regulation, defense against mobile repetitive DNA sequences and pathogen virulence (Moazed, 2009; Weiberg et al., 2015). The first evidence of double-stranded RNA (dsRNA) being a trigger for gene silencing was found in the late 1990s in *Caenorhabditis elegans* (Fire et al., 1998). DsRNA can derive from viral infections or endogenous sources e.g. transposons (Chen & Hur, 2022). RNAi is mediated by the RNA-induced silencing complex (RISC) that is programmed to target nucleic acid sequences for silencing (Pratt & MacRae, 2009).

In *Drosophila melanogaster* RNA silencing is directed by miRNAs (gene regulation) and siRNAs (defense against viruses and endogenous transposons) (Figure 1). These two classes of small RNAs are derived from double-stranded precursors through nucleolytic processing by two distinct Dicer enzymes, a dsRNA-specific RNase III family ribonuclease, working in complex with the dsRNA binding proteins Loquacious (Loqs) or R2D2 (Bernstein et al., 2001; Evers et al., 2015; Lee et al., 2004). The production of miRNAs starts with synthesis of pri-miRNAs in the nucleus. Micro RNAs originate from genomic loci that are located in intergenic regions or protein-coding genes transcribed by RNA Pol II (Dai et al., 2012; Jaubert et al., 2007). In flies, the pri-mRNAs are recognized and cleaved into hairpin RNAs (pre-miRNAs) by the microprocessor complex consisting of Drosha (RNase III family nuclease) and Pasha (RNA binding protein) (Denli et al., 2004). After the export of the pre-miRNA into the cytoplasm through a RanGTP/exportin-5-dependent mechanism, pre-miRNAs are recognized and processed by Dicer-1 into the mature miRNA (Yi et al., 2003). siRNAs can result from dsRNA from exogenous sources like RNA viruses (exo-siRNAs) or endogenous sources like dsRNAs expressed e.g. from transposable elements (endo-siRNAs). The RNA Pol II core complex synthesizes ssRNAs from transposon-coding regions which fold into dsRNA (Okamura et al., 2008). After export from the nucleus, the dsRNA is processed into the mature siRNA by Dicer-2 in complex with the D-isoform of Loqs or R2D2 (Tants et al., 2017; Tomari et al., 2004). The resulting siRNAs or miRNAs are loaded into Ago1 or Ago2, an effector endonuclease of the Argonaute-family (Cenik & Zamore, 2011; Förstemann et al., 2007; Ipsaro & Joshua-Tor, 2015). In mammals, only one Dicer-enzyme is responsible for processing of both miRNAs and siRNAs (Svobodova et al., 2016). They have two dsRNA binding proteins working together with Dicer though: TRBP and PACT which are homologs of *Drosophila* Loqs and R2D2 (Chendrimada et al., 2005; Haase et al., 2005; Lee et al., 2006). Humans have

four functional Argonaute proteins AGO1-4). Among them, AGO2 is the only essential one, it is most abundant and ubiquitously expressed (Cheloufi et al., 2010; Nakanishi, 2022). Human AGO2 as well as the other human AGO-proteins, consists of four structurally very similar domains: N-terminal-domain, PAZ-domain, Mid-domain and Piwi-domain (Elkayam et al., 2012; Nakanishi, 2022). Human AGO2 is most similar to *Drosophila* Ago1 and it localizes to P-body like structures *in vivo* (Liu et al., 2005). *Drosophila* Ago2 also consists of the four Ago-domains but additionally has a highly repetitive, glutamine-rich intrinsically disordered region at the N-terminus (Hain et al., 2010). The *C. elegans* homolog of Loqs and R2D2 is called RDE-4. In *C. elegans*, one Dicer protein and some Dicer-related helicases are involved in small RNA-mediated gene silencing as well as 27 Ago-proteins (Nakamura et al., 2007; Tabara et al., 2002; Yigit et al., 2006). One particular feature in *C. elegans* is RNAi inheritance: the progeny of animals exposed to dsRNA continue to silence genes that were targeted by dsRNA in previous generations (Spracklin et al., 2017). Inherited small RNAs are amplified by RNA-dependent RNA polymerases thus dilution is avoided and the small RNAs can persist for multiple generations (Rechavi et al., 2014). In plants, at least four distinct small RNA silencing pathways have developed to cope with different functional requirements (Baulcombe, 2004; Eamens et al., 2008). Plants have evolved multiple RNA silencing factors like for instance *Arabidopsis* which encodes four Dicer-like proteins, six RNA-dependent RNA polymerases and ten AGOs (Guo et al., 2016).

1.2 Biogenesis of small RNAs in *Drosophila melanogaster*

Micro RNA pathway

Micro RNAs (miRNAs) are a class of small non-coding RNAs of approximately 22 nucleotides (nt) in length that regulate gene expression post-transcriptionally by targeting messenger RNAs (mRNAs). This triggers the translational repression and RNA degradation (Colaianni & De Pitta, 2022). In the nucleus, the primary miRNA transcript (pri-miRNA) is processed into a 60-70 nt long pre-miRNA by Drosha (type III RNase) in complex with Pasha (dsRNA-binding protein; DGCR8 in mammals) (Colaianni & De Pitta, 2022; Kadener et al., 2009; Lee et al., 2002) (Figure 1). The pre-miRNA has a hairpin structure with a certain degree of mismatches or loops in the stem and a two nt overhang at its 3' end as well as a 5' phosphate group characteristic of RNase III cleavage products (Zeng & Cullen, 2004). Exportin-5 carries the pre-miRNA to the cytoplasm where the miRNA is processed by Dicer-1 (Lund et al., 2004; Zeng & Cullen, 2004). Dicer-1 works in complex with the B-isoform of the dsRNA-binding protein Loquacious (Loqs-PB; TRBP in mammals) (Chendrimada et al., 2005) separating the loop from the stem (Jiang et al., 2005).

Recent structural studies of Dcr-1 in complex with Loqs-PB showed that the pre-miRNA binds a rare open conformation of the Dcr-1/Loqs-PB heterodimer (Jouravleva et al., 2022). Without pre-miRNA binding, the heterodimer is predominantly present in a closed conformation. The dsRBDs of Loqs-PB form a belt around the pre-miRNA. The cleavage of the 5' and 3' end leads to the mature miRNA/miRNA* duplex. This shifts the dsRBDs and closes the conformation of Dcr-1 and thus promoting product release. The dsRBDs 1 and 2 of Loqs-PB could not be resolved yet indicating that they are mobile and available to participate in the initial binding of the RNA (Jouravleva et al., 2022). Most of the resulting miRNAs are loaded into Argonaute 1 (Ago1), an effector endonuclease of the Argonaute-family (Cenik & Zamore, 2011; Förstemann et al., 2007; Ipsaro & Joshua-Tor, 2015). GW182, an RNA-binding protein, localizes Ago1 to P-bodies where mRNA targets are decayed or stored. P-bodies are membrane-less organelles formed through liquid-liquid phase separation (LLPS) and serve as a center for RNA turnover (Eulalio et al., 2007). Binding of Dcr-1/Loqs-PB to Ago1 and the association with GW182 happens in a mutually exclusive manner and Ago2 does not interact with GW182 (Miyoshi et al., 2009).
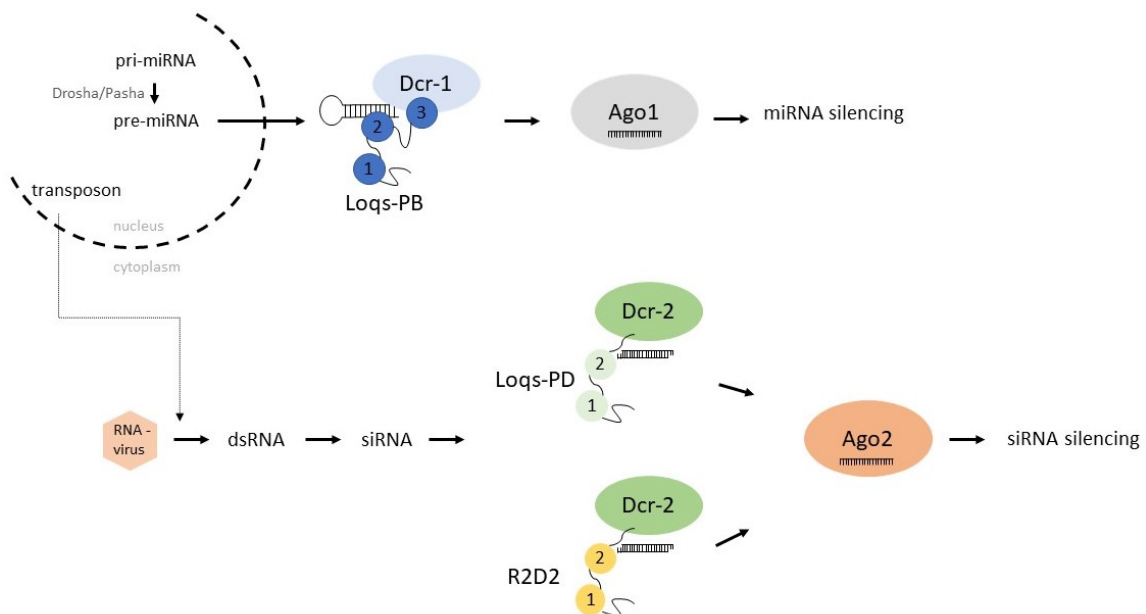

Figure 1. Overview of the distinct small RNA silencing pathways in Drosophila melanogaster. The double-stranded RNA binding domains of Loqs-PB (dark blue), Loqs-PD (light green) and R2D2 (yellow) are numbered.

Small interfering RNA pathway

Small interfering RNAs (siRNAs) derive from long double-stranded precursors. They can be introduced into a cell from exogenous sources e.g. during the replication of an RNA virus or endogenously when derived from transposons (Czech et al., 2008; Golden et al., 2008). In the cytoplasm, the dsRNA is processed by a complex of Dcr-2 and R2D2 or its paralog, the D-isoform of Loqs (Loqs-PD) (Hartig et al., 2009; Tants et al., 2017; Tomari et al., 2004). After processing of the dsRNA by the complex of Dcr-2/R2D2 or Dcr-2/Loqs-PD, the siRNAs are loaded into Ago2 (Ghildiyal & Zamore, 2009). An alternative model by Richard W. Carthew and colleagues, developed based on observations made in flies, suggests that Loqs and R2D2 function sequentially and non-redundantly in complex with Dcr-2. They propose that dsRNA is processed by Dcr-2/Loqs and the resulting siRNAs are sorted and loaded into Ago2-RISC (RNA-induced silencing complex) by Dcr-2/R2D2 (Marques et al., 2010). In cultured S2-cells, the complex of Dcr-2 and R2D2 senses the asymmetry of exo-siRNAs and serves as the RISC loading complex (RLC) that loads the exo-siRNA into Ago2 (Liu et al., 2006; Tomari et al., 2004). Loqs-PD is required for the production of endo-siRNAs (Zhou et al., 2009). Dcr-2 and R2D2 have been shown to colocalize to cytoplasmic foci called D2-bodies (Nishida et al., 2013). Due to solubility issues of R2D2 when not in complex with Dcr-2, it is challenging to examine R2D2 *in vitro* whereas its paralog Loqs-PD can be purified and studied individually. The partial redundancy of R2D2 and its paralog Loqs-PD has been demonstrated through biochemical experiments and further supported by deep sequencing experiments that showed that even in *r2d2* null mutant animals, some Ago2-loaded siRNAs are present (Marques et al., 2010; Mirkovic-Hosle & Forstemann, 2014; Nishida et al., 2013). Loqs-PD can replace R2D2 for the loading of exo- and endo-siRNAs into Ago2 by serving as a siRNA asymmetry sensor for an alternative RLC. The combined action with Dcr-2 is essential for the strand discrimination (Tants et al., 2017). The selection of the guide strand is determined by the orientation and thermodynamic asymmetry of the siRNA duplex. The thermodynamically less stable 5'end of the double-stranded small RNA determines its fate as small RNA guide strand whereas the other strand becomes the passenger strand. As soon as the siRNA passenger strand of the small RNA duplex is evicted from the pre-RISC, that is formed by Ago2 binding to the siRNA duplex, the complex becomes the mature RISC. After the base pairing of the guide siRNA to the cognate target mRNA, the passenger strand is degraded by Ago2 (Cenik & Zamore, 2011; Pham et al., 2004). The detection of fully complementary sequences within target RNAs by the RISC result in Ago2-mediated cleavage of the RNA target (Schwarz et al., 2002).

Cryo-EM-based structural studies recently revealed the molecular mechanism for the ATP-dependent dsRNA processing by Dcr-2 in complex with Loqs-PD (Su et al., 2022). In absence of ATP, Dcr-2/Loqs-PD tends to dimerize and forms an initial binding complex with dsRNA. ATP-dependent conformational changes are required for the formation of the active dicing state to cleave the dsRNA into a 21 base pair siRNA duplex. Only the structure of the C-terminus of Loqs-PD has been resolved so far in complex with Dcr-2 since the other portions of the protein cannot be distinguished probably due to its flexible nature. Binding of dsRNA to Dcr-2 induces a conformational change of the helicase and DUF283 domains from a stretched conformation to a closed one wrapping around the RNA helix. During the translocation of Dcr-2/Loqs-PD along the dsRNA, the RNA duplex threads through the helicase domain towards the catalytic center of Dcr-2. In the active dicing state, the PAZ-domain binds the terminus of the dsRNA through the recognition of the 3' two-nucleotide overhang and the 5'-phosphate, respectively. Near the catalytic center, the cleavage of the dsRNA was observed exactly 21 nt away from the PAZ-domain-binding terminus. This cleavage of the dsRNA disrupts the binding site for the C-terminal dsRBD in the active dicing state and the siRNA product is released (Su et al., 2022).

Loqs-PD has only two dsRBDs whereas Loqs-PB has three although Loqs-PB dsRBD3 does not bind RNA but appears to interact with Dcr-1 (Jakob et al., 2016). The dsRBDs of both Loqs isoforms are connected by unstructured linkers (Förstemann et al., 2005; Tants et al., 2017). The N-terminus of Loqs-PD is Q/N-rich and a PLAAC-predicted prion-like domain (Figure 2) (Lancaster et al., 2014).


```
  1  MDQENFHGSSLPQQLQNLHIQPQQASPNPVQTGFAPRRHYNNLVGLGNGNAVSGSPVKGAPLGQRHVKLKKEKISAQVAQLSQPGQLQLSDVGDPALAGG
101  SGLQGGVGLMGVILPSDEALKFVSETDANGLAMKTPVSILQELLSRRGITPGYELVQIEGAIHEPTFRFRVSFKDKDTPFTAMGAGRSKKEAKHAAARAL
201  IDKLIGAQLPESPSSSAGPSVTGLTVAGSGGDGNANATGGGDASDKTVGNPIGWLQEMCMQRRWPPPSYETETEVGLPHERLFTIACSILNYREMGKGKS
301  KKIAKRLAAHRMWMRLQETPIDSGKISDSICGELEGEVSIIQDIDRYEQVSKDFEFIKI
```

Figure 2: PLAAC-prediction of Loqs-PD N-terminus as prion-like domain. Amino acid sequence of Loqs-PD from Flybase (FB2023_02) below. (Lancaster et al., 2014)

Ago2 is a modular protein consisting of a N-terminal domain, PAZ-domain, Mid-domain and Piwi-domain in the carboxyterminal half of the protein (Hain et al., 2010; Nakanishi, 2022). The N-terminal domain of Ago2 is highly repetitive, glutamine- and asparagine-rich and shows features

of disordered prion-like domains (Figure 3). The glutamine-rich and prion-like property of Ago2 N-terminus is evolutionary conserved (Hain et al., 2010; Palmer & Obbard, 2016).


```
   1 MGKKDKNKKGGQDSAAAPQPQQQQKQQQQRQQQPQQLQQPQQLQQPQQLQQPQQQQQQQPHQQQQQSSRQQPSTSSGGSRASGFQQGGQQQKSQDAEGWT
 101 AQKKQGKQQVQGWTKQGQQGGHQQGRQGQDGGYQQRPPGQQQGGHQQGRQGQEGGYQQRPPGQQQGGHQQGRQGQEGGYQQRPSGQQQGGHQQGRQGQEG
 201 GYQQRPPGQQQGGHQQGRQGQEGGYQQRPSGQQQGGHQQGRQGQEGGYQQRPPGQQQGGHQQGRQGQEGGYQQRPPGQQQGGHEQGRQGQEGGYQQRPSG
 301 QQQGGHQQGRQGQEGGYQQRPSGQQQGGHQQGRQGQEGGYQQRPSGQQQGGHQQGRQGQEGGYQQRPPGQQPNQTQSQGQYQSRGPPQQQQAAPLPLPPQ
 401 PAGSIKRGTIGKPGQVGINYLDLDLSKMPSVAYHYDVKIMPERPKKFYRQAFEQFRVDQLGGAVLAYDGKASCYSVDKLPLNSQNPEVTVTDRNGRTLRY
 501 TIEIKETGDSTIDLKSLTTYMNDRIFDKPMRAMQCVEVVLASPCHNKAIRVGRSFFKMSDPNNRHELDDGYEALVGLYQAFMLGDRPFLNVDISHKSFPI
 601 SMPMIEYLERFSLKAKINNTTNLDYSRRFLEPFLRGINVVYTPPQSFQSAPRVYRVNGLSRAPASSETFEHDGKKVTIASYFHSRNYPLKFPQLHCLNVG
 701 SSIKSILLPIELCSIEEGQALNRKDGATQVANMIKYAATSTNVRKRKIMNLLQYFQHNLDPTISRFGIRIANDFIVVSTRVLSPPQVEYHSKRFTMVKNG
 801 SWRMDGMKFLEPKPKAHKCAVLYCDPRSGRKMNYTQLNDFGNLIISQGKAVNISLDSDVTYRPFTDDERSLDTIFADLKRSQHDLAIVIIPQFRISYDTI
 901 KQKAELQHGILTQCIKQFTVERKCNNQTIGNILLKINSKLNGINHKIKDDPRLPMMKNTMYIGADVTHPSPDQREIPSVVGVAASHDPYGASYNMQYRLQ
1001 RGALEEIEDMFSITLEHLRVYKEYRNAYPDHIIYYRDGVSDGQFPKIKNEELRCIKQACDKVGCKPKICCVIVVKRHHTRFFPSGDVTTSNKFNNVDPGT
1101 VVDRTIVHPNEMQFFMVSHQAIQGTAKPTRYNVIENTGNLDIDLLQQLTYNLCHMFPRCNRSVSYPAPAYLAHLVAARGRVYLTGTNRFLDLKKEYAKRT
1201 IVPEFMKKNPMYFV
```
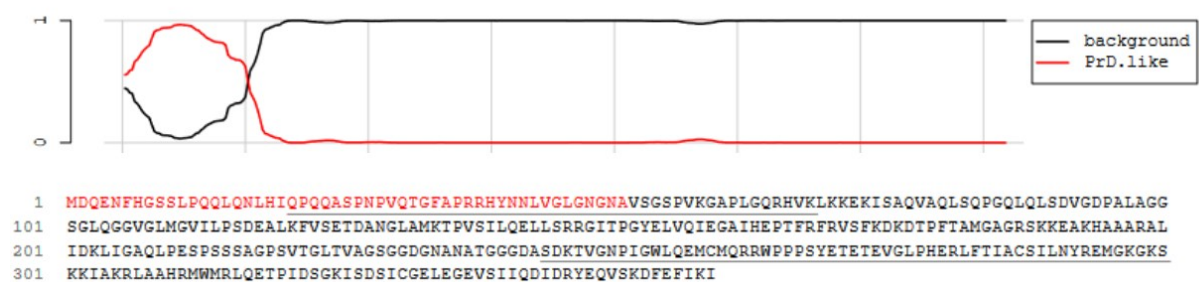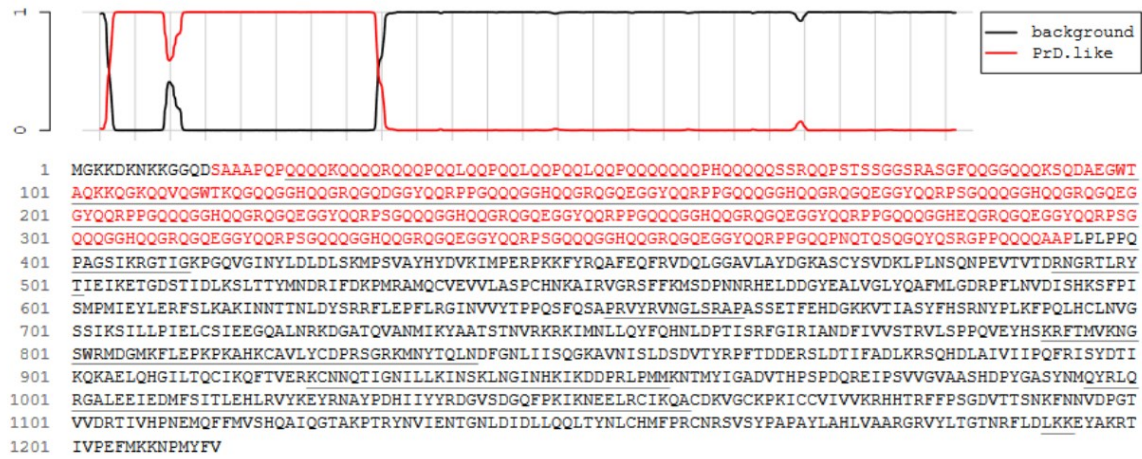
Figure 3. **PLAAC-prediction of Ago2-PB N-terminus as prion-like domain.** Amino acid sequence of Ago2-PB from Flybase (FB2023_02) below. (Lancaster et al., 2014)

Piwi-interacting RNA pathway

The Piwi-interacting RNA (piRNA) biogenesis is distinct from the other small RNA silencing pathways since it is a Dicer-independent pathway. With 23-29 nt of length, piRNAs are the longest ones of the small RNA regulatory classes (Aravin et al., 2003). Together with Piwi-proteins, they are required for the suppression of transposable elements in the germline and somatic tissue of the *Drosophila* ovary (Aravin et al., 2001; Malone et al., 2009). piRNAs are produced in a Dicer-independent manner by the Piwi-family proteins Piwi, Aubergine (Aub) and Ago3 in the germ cells and Piwi only in the somatic cells (Malone et al., 2009). Once the piRNA precursors that arise from transcripts of e.g actively expressed transposons have been exported from the nucleus to the cytoplasm, the mature piRNA is further processed through a ping-pong amplification loop in germ cells (Aravin et al., 2007; Brennecke et al., 2007; Huang et al., 2017). Precursor piRNAs (anti-sense strands) are loaded onto Aub. The Aub-bound anti-sense piRNA targets the sense transposon transcript and slices their 5' end to produce sense piRNAs. The 3' ends of the sense piRNAs are then loaded onto Ago3 to sense the piRNA target and process the precursor anti-sense piRNA into mature piRNAs to start the cycle again by loading this piRNA onto Aub. Proteins involved in piRNA biogenesis localize to a cytoplasmic compartment called nuage (germline-specific perinuclear granules) (Lim & Kai, 2007; Pek et al., 2012). The protein Krimp can form granules independently from other nuage proteins and recruits piRNA-loaded

Aub and unloaded Ago3 to form a complex (Soleimani et al., 2020). In addition to the perinuclear nuage, Aub and Ago3 can be found in cytoplasmic foci (P-bodies) during oogenesis (Lim et al., 2009). Both, the nuage and piRNA pathway components, colocalize with P-bodies that further include retroelement transcripts, anti-sense piRNAs and proteins involved in mRNA degradation (Pek et al., 2012).

1.3 Liquid-liquid phase separation in cells

The phenomenon of phase separation can be described by a homogeneous liquid solution (phase) of macromolecular components separating or de-mixing into two distinct phases. One of the phases is enriched for the macromolecules and the other phase is depleted of those (Alberti et al., 2019; Banani et al., 2017; Brangwynne et al., 2015; Hyman et al., 2014). LLPS within aqueous solutions can serve as a phenomenon to spatially organize biochemical reactions without the need for a membrane barrier in contrast to organelles that are surrounded and separated by lipid bilayer membranes (Banani et al., 2017). Phase separation can augment reaction efficiencies due to high local substrate and enzyme concentrations. It can be essential for signal processing and transmission events that the required signaling molecules coalesce into an induced separated phase (Shin & Brangwynne, 2017; Wheeler & Hyman, 2018; Wu, 2013). The concentration and properties of the macromolecules as well as environmental conditions like temperature, salt type and concentration, co-solutes and pH can determine whether a solution undergoes phase separation (Franzmann & Alberti, 2019a; Nott et al., 2015; Ruff et al., 2018). When solutions of macromolecules undergo LLPS they condense into a dense phase that resembles droplets that exhibit a spherical shape with surface tension and a certain viscosity. The viscosity describes the motion of a liquid under external force whereas surface tension is a static property. The viscosity of a condensate can be assessed by fluorescence recovery after photobleaching (FRAP, see below) or single particle tracking. Both of these techniques are based on the Stokes-Einstein relation, where the viscosity of a liquid is inferred from the Brownian motion of spherical particles within it (Bracha et al., 2019; Schuster et al., 2021). Measurements of the surface tension rely on the scaling between fusion time and the length scale of two coalescing droplets (Schuster et al., 2021).

To examine the conditions under which a system undergoes phase separation, one can generate phase diagrams by experiments that define the set of conditions that results in a single, well mixed phase and the conditions that promote the phase separation (Figure 4) (Alberti et al., 2019). At concentrations below c_{sat}, the system is in a one-phase regime (Figure 4, bottom). In a

two-phase regime, so-called tie lines result from connecting the light-phase and dense-phase concentrations under given conditions. Within the two-phase regime, the system demixes into a light phase (with $c = c_L$) and a dense phase (with $c = c_D$) at any condition. All conditions on the tie line result in a two-phase system with fixed light-phase and dense-phase concentrations for c_L and c_D, only the volume fractions change relatively to each other (Figure 4) (Alberti et al., 2019).
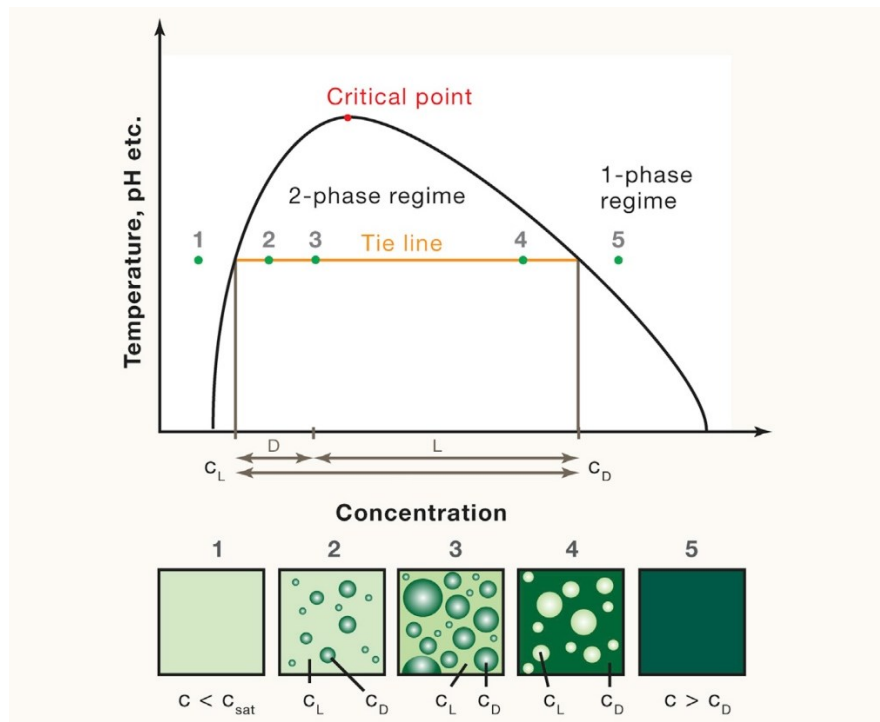

Figure 4. Schematic phase diagram and an interpretative drawing below. Adapted from Alberti et al., 2019.

The solubility of macromolecules depends on the balance between the weak interactions between macromolecules and those with the solvent (water in biology) (Banani et al., 2017). A concept to describe how components get enriched in condensates is the concept of scaffolds and clients (Banani et al., 2016). Scaffold proteins are driving the formation of condensates and they are thus critical for the emergence of condensates. They are often present at high concentrations and have many valencies. Multivalent molecules harbor multiple elements that govern intra- or intermolecular interactions (Li et al., 2012). This multivalency is important because multivalent molecules naturally assemble into large oligomers or polymers when mixed. This assembly decreases the solubility of the molecule due to entropy-driven effects and by this promotes their phase separation (Flory, 1953). Moreover, scaffolds are able to phase

separate at their physiological concentrations while client proteins phase separate at non-physiologically high concentrations and they form phase-separated liquids that concentrate these low valency client proteins (Banani et al., 2017; Banani et al., 2016; Wang et al., 2017). On the molecular level one can discriminate between two types of phase separating proteins: 1) proteins with multiple folded domains and 2) intrinsically disordered proteins (IDP) or proteins with intrinsically disordered regions (IDR) (Alberti et al., 2019; Banani et al., 2017). Multidomain proteins carry several folded protein-protein interaction domains connected by flexible linkers (Li et al., 2012; Su et al., 2016). These interaction domains frequently interact with short linear motifs in other proteins. The more modules a protein has, the higher is its valence and therefore the propensity to phase separate (Li et al., 2012). As their name implies, IDRs and IDPs have no folded native conformation. They can be described as polymers consisting of two units: stickers and spacers. Stickers in folded protein domains are surfaces patches or motifs that emerge from the formation of specific structures. Non-sticker regions and disordered loop regions can be considered as spacers. Stickers provide interactions whereas the spacer regions promote conformational flexibility. Additionally, stickers provide a specific amino acid chemistry that encodes the driving forces and specificity of condensate formation (Wang et al., 2018). IDRs can be classified on the basis of their sequence composition and motifs like fraction and patterning of charged residues. One class of IDRs are those containing arginine-rich and glycine-rich (RGG/RG) repeats (Chong et al., 2018; Thandapani et al., 2013). IDRs that contain RGG/RG-motifs can self-interact but also associate with RNA to promote the formation of RNA-containing condensates. RNA plays a major role in condensate formation especially in ribonucleoprotein granules. Because of its long length, flexibility and multivalency, RNA is an ideal scaffold molecule to provide binding sites to proteins in the cytoplasm (Alberti & Dormann, 2019). Therefore, co-condensates of RNA with proteins are frequently observed. Another class of IDRs are prion-like domains that are enriched in repetitive sequences of only a few of the 20 possible amino acids (such as glutamine, asparagine, serine, tyrosine), resulting in domains of low complexity (Alberti et al., 2009; Duster et al., 2021). Prion-like RNA binding proteins use a specific protein intrinsic grammar to drive the formation of condensates. This involves interactions between tyrosine and arginine residues. They are the stickers that determine the saturation concentration and are connected by spacer residues (Wang et al., 2018).

Methods for examining the liquid-like nature of a condensed phase

Key insights into the role of phase transitions came from studies in *C. elegans* where P-granules (RNA and protein-rich bodies) have been described via time-lapse microscopy as spherical shapes being able to fuse into larger droplets when in contact with one another and are critically influenced by the surface tension. They also exhibit wetting and dripping behaviors that are hallmarks of a liquid-like behavior. Furthermore, when one half of a given droplet was bleached, FRAP was observed suggesting a rapid diffusion inside the granule (Brangwynne et al., 2009). FRAP is widely used to assess condensate fluidity and to estimate diffusion coefficients. Condensates can freely exchange components with their surroundings. This exchange can be demonstrated using FRAP. During a FRAP experiment, a defined region of interest is bleached irreversibly. The recovery of the fluorescent signal in the bleached area results from the exchange of bleached and unbleached condensate. The kinetics of the recovery give an indication of the protein mobility. A faster recovery suggests a higher diffusion coefficient (Taylor et al., 2019). Besides the FRAP assay, hexanediol, an aliphatic alcohol, can be used to differentiate between liquid-like and solid-like assemblies and to examine physical properties of membrane-less organelles *in vivo*. Hexanediol can dissolve dynamic assemblies like P-granules through inhibiting weak hydrophobic protein/protein-RNA interactions whereas solid-like assemblies such as protein aggregates or cytoskeletal assemblies are resistant (Kroschwald et al., 2017). Another reagent that is frequently used to examine liquid-like properties of cytoplasmic foci is ammonium acetate that can dissolve charge-based interactions (Jain & Vale, 2017). These treatments can be used to demonstrate that the formation of condensates is reversible.

1.4 Aberrant phase transitions can cause disease

The aggregation of proteins can become critical for an organism when it results from aberrant phase transitions. Diseases can arise from genetic mutations or environmental perturbations that alter the mechanism of assembly, the activity of a critical regulator of phase separation or the chemical and physical conditions inside a cell (Alberti & Dormann, 2019). Genetic mutations can affect the valence of a scaffold or a client protein. Parameters like size, number or morphology of a condensate could be affected from mutations in a sticker region of a scaffold protein that change the interactions between the molecules. Mutations in the sequence of a client protein could lead to changes in the partition coefficient that results in mislocalization. Besides mutations that alter the valence of a protein, there could be mutations that alter the

material properties of condensates. Mutations in spacer regions could lead to conformational changes of the protein that affect the material properties of a condensate with potential gain- and loss-of-function defects. Another example for mutations that could affect the formation of condensates would be mutations that inactivate an enzyme regulating the condensate formation. This could be changes of expression levels of a key nucleator of a condensate that lead to the formation of ectopic condensates or altered activity levels of e.g. a kinase that normally adapts a protein phase to changing conditions in a cell. Physiochemical conditions inside a cell can be changed by genetic changes as well. The formation of condensates is regulated by an active energy-consuming process. Hence, mutations in the energy metabolism could change the normal ATP levels in cells and result in aberrant condensate formation (Alberti & Dormann, 2019). Cell-internal conditions like pH, osmotic pressure or salt concentration are required to be stable for normal condensate formation (Franzmann & Alberti, 2019b; Rabouille & Alberti, 2017). Thus, change of these conditions can lead to excessive phase separation or altered material properties of a condensate.

Disease-causing phase separation behavior can lead to cancer as well as infectious diseases or neurodegenerative diseases. Prion-like IDPs such as FUS and TDP-43 are involved in the formation of RNA-containing compartments in the cytoplasm and nucleus and are associated with the neurodegenerative disease ALS (amyotrophic lateral sclerosis) (Patel et al., 2015; Polymenidou et al., 2012). Prion-like domains are uncharged with recurrent aromatic residues and they are very flexible which makes these domains very interactive. In late stages of ALS, these proteins from pathological aggregates (Patel et al., 2015; Polymenidou et al., 2012). The pathological inclusions of FUS and TDP-43 contain additional RBPs like stress granules (Bentmann et al., 2012; Liu-Yesucevitz et al., 2010). Observations like these suggest that compartments such as stress granules can change their physical properties and mature into pathological aggregates (Alberti & Hyman, 2016). Initially, FUS forms liquid-like assemblies which fuse and recover quickly after photobleaching. With time, their dynamic properties change and they stop fusing and show slower recovery during FRAP assay (Murakami et al., 2015; Patel et al., 2015). The material property of these assemblies can be described as hydrogel-like (Kato et al., 2012). Finally, they can also convert into solid-like fibrillar aggregates. Therefore, there seems to be a driving force for IDPs in liquid-like compartments to form solids with time (Alberti & Hyman, 2016). There have been mutations identified in ALS-patients that increase the propensity of phase separating proteins also to convert to a solid state spontaneously. For TDP-43, most of the mutations were mapped to its intrinsically disordered

C-terminal domain that drives the phase separation behavior of this protein (Li et al., 2013). FUS also forms solids more rapidly when mutated in the prion-like domain (Lin et al., 2015; Patel et al., 2015). In young cells an active metabolism controls the tendency of these proteins to aggregate. With age, processes of the metabolism such as mitochondrial function decline and homeostasis mechanisms can get out of balance. When mitochondrial activity starts to decline, the metabolic potential of cells decreases and triggers a loss of homeostasis and aberrant phase transitions. Aberrant phase separation could also be a driver that accelerates the aging process and could cause age-related diseases (Alberti & Hyman, 2016).

1.5 Aim of this thesis

The aim of the thesis was to decipher the role of liquid-liquid phase separation of Loqs-PD, Dcr-2 and dsRNA during RISC-loading. R2D2, a Loqs-PD paralog, co-condensates with Dcr-2 in membrane-less organelles, so-called D2-bodies (Nishida et al., 2013). We hypothesize that Loqs-PD and Dcr-2 can form condensates together as well and that Ago2 could be part of these condensates either as a scaffold or as a transient. The N-terminal regions of Loqs-PD and Ago2 are predicted to be low complexity intrinsically disordered domains. Furthermore, Loqs-PD contains two double-stranded RNA binding domains. The multi-valent interaction possibilities of the folded domain as well as the intrinsically disordered domain, the ability to bind to nucleic acids and the possible scaffold/client configuration that can be observed in Ago2 and Loqs-PD are typical features for proteins undergoing liquid-liquid phase separation (Berry et al., 2018; Polymenidou, 2018). Therefore, the phase-separation behavior of the key-proteins for siRNA silencing Loqs-PD, Dcr-2 and Ago2 and their potential colocalization was examined *in vivo*.

2 Results

2.1 The role of the dsRBD2 for condensate formation of Loqs-PD

Genomic engineering of S2 cells to generate a r2d2 and loqs double knockout clone

The goal was to generate a *r2d2* and *loqs* double knockout clone in S2-cells to use it for complementation assays with various Loqs-constructs. Since the generation of a double knockout had been unsuccessful in the past, the new attempt was to generate a cell line with inducible Loqs in an already existing *r2d2* knockout cell line (Tants et al., 2017). By replacing the endogenous *loqs*-promoter with an expression cassette including a metallothionine-promoter and a 3xFLAG-tag, it is possible to induce Loqs-expression by adding $CuSO_4$ to the cell culture medium or to not induce the Loqs-expression by not adding $CuSO_4$ (Figure 5). Like this, one would keep the *loqs* expression during selection to circumvent the problem that the cells do not grow properly in a double-knock-out situation. Not adding $CuSO_4$ would create a system where Loqs is not expressed in the background of the *r2d2* knockout cell line and thus both proteins would be simultaneously absent. Genomic engineering was achieved by using the CRIPR/Cas9 system adapted for S2-cells by the Förstemann lab (Kunzelmann et al., 2016). By following this protocol an expression cassette including a mtnDE promoter, 3xFLAG-tag and blasticidin resistance (for the selection of successfully tagged cells) was introduced. The resulting single cell clone was named clone K54.
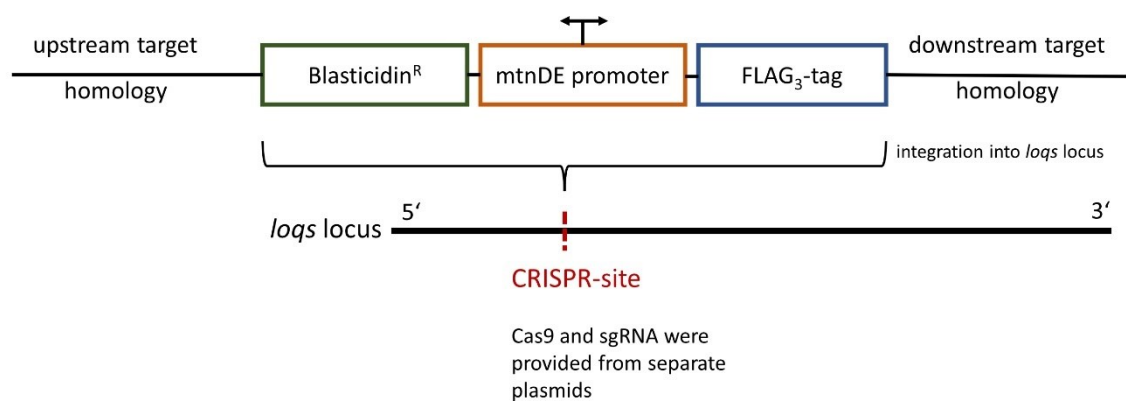

homology donor cassette:

upstream target homology — Blasticidin^R — mtnDE promoter — FLAG$_3$-tag — downstream target homology

integration into *loqs* locus

loqs locus 5' 3'

CRISPR-site

Cas9 and sgRNA were provided from separate plasmids

Figure 5. Schematic drawing of the homology donor cassette. A blasticidin resistance, the mtnDE promoter and a FLAG-tag are inserted at the CRIPSR-targeted site in the *loqs* locus. The sgRNA and Cas9 were provided from separate plasmids.

As shown in Figure 6, it was still not possible to generate a single cell clone where the Loqs-expression was switched off completely. Various analyses showed that there was some expression left in the uninduced state. Figure 6A shows an anti-Loqs western blot with isolated protein (isolated with 8M urea) of wild type cells and clone K54 induced with 10 µM CuSO₄. A titration experiment showed that induction with 10 µM CuSO₄ resembles the wild type Loqs expression level and thus was chosen for inducing Loqs-expression in clone K54 for all of the experiments (Figure 6 B). The western blot in Figure 6A depicts the total isolated protein of wild type cells in the left lane where the three bands for Loqs are visible. A rabbit polyclonal antibody raised against dsRBD2 of Loqs was used. This antibody detects three isoforms of the endogenous Loqs, the Loqs-D-isoform being the smallest band of these three (Tants et al., 2017). Clone K54 induced with 10 µM CuSO₄ (right lane) shows the same three Loqs-isoforms as visible in the wildtype with a slight size-shift due to the FLAG-tag. In the uninduced state (middle lane), there is only one faint band visible being remaining protein expression of Loqs-PD.

Figure 6B shows a 1%-agarose gel with genomic DNA isolated from wild type cells and clone K54. A PCR product around 600 nt (nucleotides) corresponds to the expected size of an untagged *loqs* wt-allele. A band of 600 nt size is visible in the wild type and clone K54. The 600 nt fragment, diagnostic of a wild-type allele, confirms incomplete modification of the loqs-locus in clone K54. A PCR product around 2000 nt corresponds to the expected size of tagged *loqs* alleles. Besides the tagged *loqs*-alleles there are still wild type alleles left in clone K54. The control PCR (water control) with water instead of DNA in the reaction mixture showed unspecific bands of various sizes. Figure 6D shows the fold change of RNA levels of clone K54 induced or uninduced relative to the wild type and normalized to the reference gene *rp49* during qPCR. Two different primer pairs were used. One primer pair targeted all *loqs* isoforms (Figure 6D, blue bars) and the other one was specific for the D-isoform (Figure 6D, grey bars). The cells were induced with 10 µM which was the concentration determined to be most similar to wildtype endogenous expression levels on a western blot (Figure 6B). In the qPCR-results, a 4- to 8-fold change was detected for the *loqs* isoform-unspecific primer pair (blue) or D-isoform specific primer pair respectively (grey) relative to the wildtype. For the uninduced sample, a 0.5- or 0.75-fold change was detected for the *loqs* isoform-unspecific primer pair (blue) or D-isoform specific primer pair respectively (grey) relative to the wildtype. These results show that the gene was downregulated in the uninduced clone K54 only partially and the expression cannot be switched off completely by culturing the cells without CuSO₄. The CRISPR-cut made to promote homology-directed repair for the editing could have been repaired by end-joining as well. This could lead to an allele that

can still make RNA but for example lack the AUG for translation. Hence, the effect on the protein-levels can be stronger than the effect on the mRNA level due to the genome editing approach used here. Taken together, these results suggest that clone K54 is the best cell line I was able to generate and therefore it has been used for the live cell imaging experiments. Additionally, the cell line served as starting cell line for the generation of stable cells but not for more sensitive experiments like small RNA library deep sequencing or qPCR since the difference between the uninduced state and induced state or wild type cells is negligible.
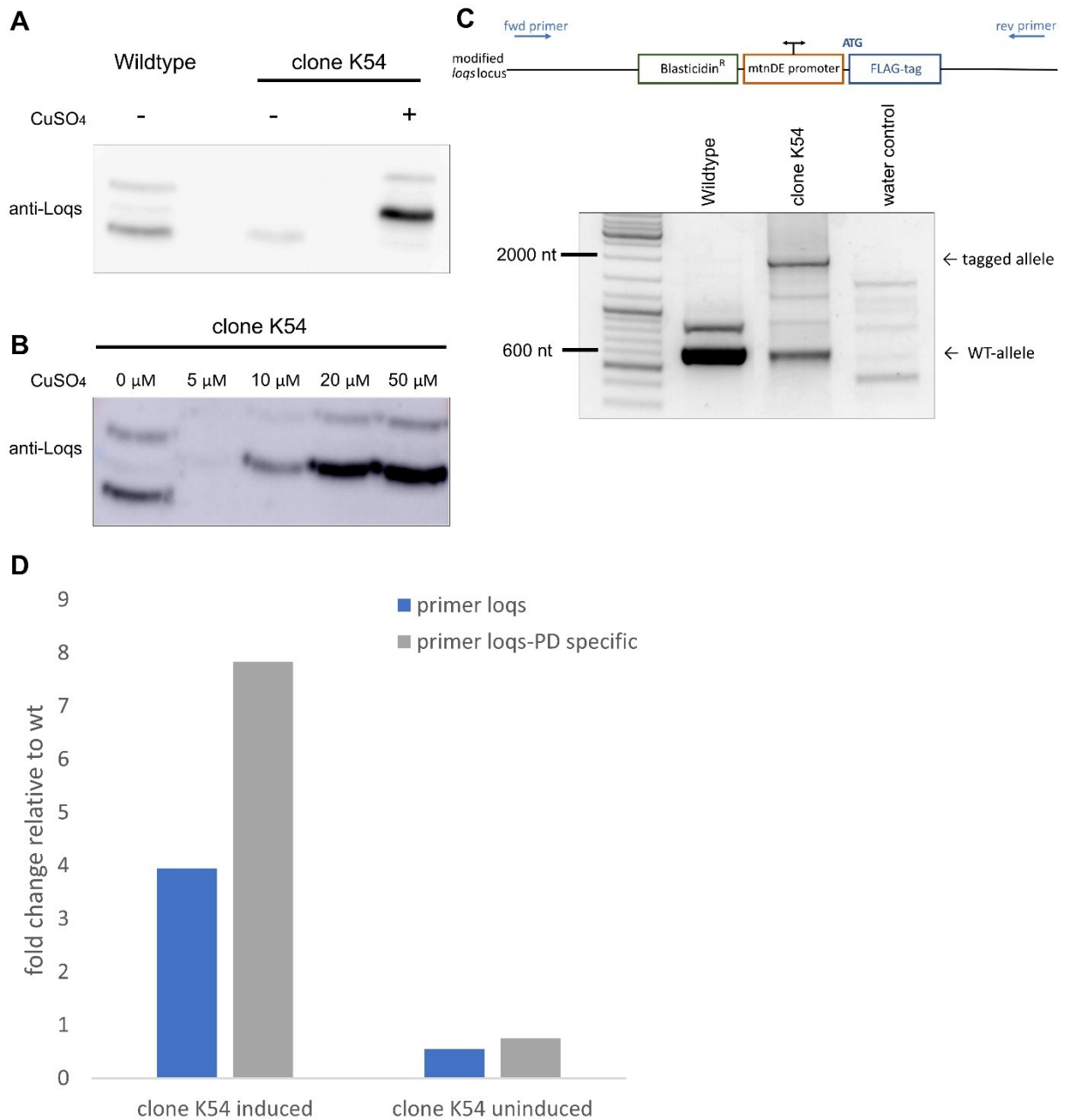
Figure 6. Characterization of clone K54 (inducible *loqs* in *r2d2* ko background). (A) Western blot (anti-Loqs) of wild type cells and clone K54 with (10 μM) or without Loqs induction (4 biological replicates). (B) Western blot (anti-Loqs) of clone K54 uninduced or induced with 5 μM, 10μ M, 20 μM or 50 μM CuSO₄. (C) Schematic drawing of modified *loqs* locus. Position of PCR-primers indicated by blue arrows. Below: PCR of genomic DNA isolated from wild type cells, clone K54 (and water control without DNA) on a 1%-agarose-gel. (D) qPCR results fold change of clone K54 induced or uninduced relative to the wildtype for a Loqs-PD specific primer pair (grey) and Loqs isoform-unspecific primer pair (blue); technical triplicate.

Small RNA profile analysis via deep sequencing

In *Drosophila*, small RNAs are sorted either into Ago1 (miRNAs) for the regulation of fly gene expression or Ago2 (siRNAs) for self-defense against RNA viruses or transposable elements(Okamura et al., 2004). Ago2-loaded small RNAs are methylated at their 2'OH of the ribose at their 5' end. Hence, Ago2-loaded siRNA guide strands are resistant to oxidation with periodate (IO_4^-) (Ji & Chen, 2012). The unmethylated 2'OH of Ago1-loaded small RNAs is oxidized by periodate which results in the opening of the ribose ring (Figure 7). Due to the oxidation and opening of the ribose ring, the linker oligonucleotide cannot be ligated to the small RNA during deep sequencing library generation. Thus, Ago1-loaded small RNAs are depleted while Ago2-sorted siRNAs are resistant and hence enriched in the sequencing library.
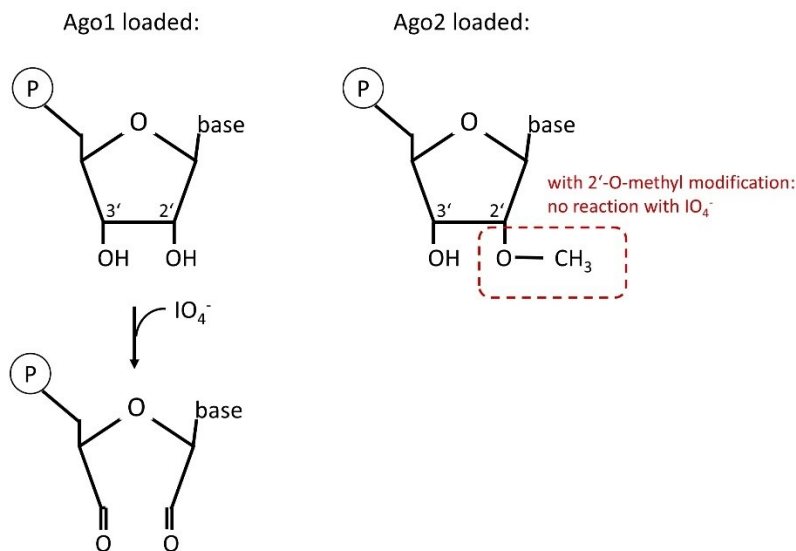

Figure 7. Chemical nature of the 3' end of small RNAs loaded either into Ago1 or Ago2. The oxidation by periodate results in the opening of the ribose ring of Ago1 loaded small RNAs whereas Ago2 loaded small RNAs are resistant to the oxidation through a 2'-O-methyl modification at their 5' end.

The initial goal was to assess the loading efficiency of Ago1 and Ago2 with various Loqs variants in *loqs/r2d2* double knockout cells. To this end, total RNA was extracted and treated or not with periodate (oxidation) from wild type cells (Figure 8), *r2d2* knockout cells (Figure 9A) and *loqs* knockout cells (Figure 9B) to generate data for control conditions. Small RNAs were isolated from the total RNA extract and these 19-25 nt long reads were sequenced, mapped to the genome and normalized to the genome matching reads. The analysis of the deep sequencing of the small RNA library of wild type cells shows the effect of prior oxidation of the RNA (Figure 8). Since

Ago2-loaded siRNA are resistant to periodate-mediated oxidation, their abundance should be comparable in the oxidized and the untreated library. Indeed, after normalizing for differences in sequencing depth, one can observe that the transposon-targeting siRNAs (grey) once mapped to the collection of transposable element consensus sequences and quantified for each transposon, fall roughly onto a diagonal line in a log-log plot. In contrast, miRNAs are depleted from the library derived from oxidized RNA and the corresponding reads, once mapped to and quantified for each miRNA (black), lie well below the diagonal in most cases.
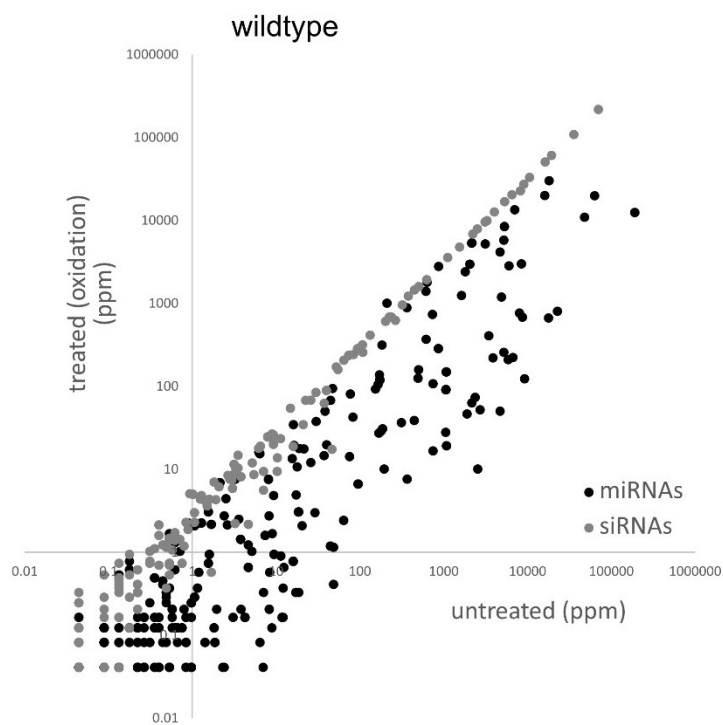

Figure 8. Deep sequencing analysis of small RNA library of treated (oxidation) or untreated RNA of wild type cells. Normalized to genome matching reads.

The same is true for the small RNAs of *r2d2* knockout and *loqs* knockout cells respectively. As shown in Figure 10 there is a difference between treated and untreated RNA. The *r2d2* knockout (Figure 9A) resembles the wildtype. This suggests that the single knockout of *r2d2* does not affect the loading efficiency of Ago2 with siRNAs. The *loqs* knockout shows only a weak effect (Figure 9B). Compared to the wildtype the curve is shifted slightly towards the x-axis. This weak effect should be investigated in more detail with a *r2d2/loqs* double knockout cell line since *r2d2* is a paralog of *loqs* and they may be able to cover for each other's function if one of them is

knocked out. For the double knockout I expected a strong effect on the loading efficiency of Ago2 and clear difference to the wildtype small RNA profile. Since there is still residual endogenous Loqs protein in clone K54 the analysis of the deep sequencing results of clone K54 did not show a big difference to wildtype, *r2d2* single knockout or *loqs* single knockout cells (Figure 9). In flies, it has been shown that without R2D2, endo-siRNAs were misdirected to Ago1 and that R2D2 and Loqs act sequentially (Marques et al., 2010). In a *r2d2/loqs* double knockout cell line, we thus would hypothesize that siRNAs will be redirected and misloaded (at least partially) into Ago1. Unfortunately, this effect was not observed here: although the Loqs-levels are low, the remaining activity suffices for Ago2 loading of transposon-derived siRNAs.
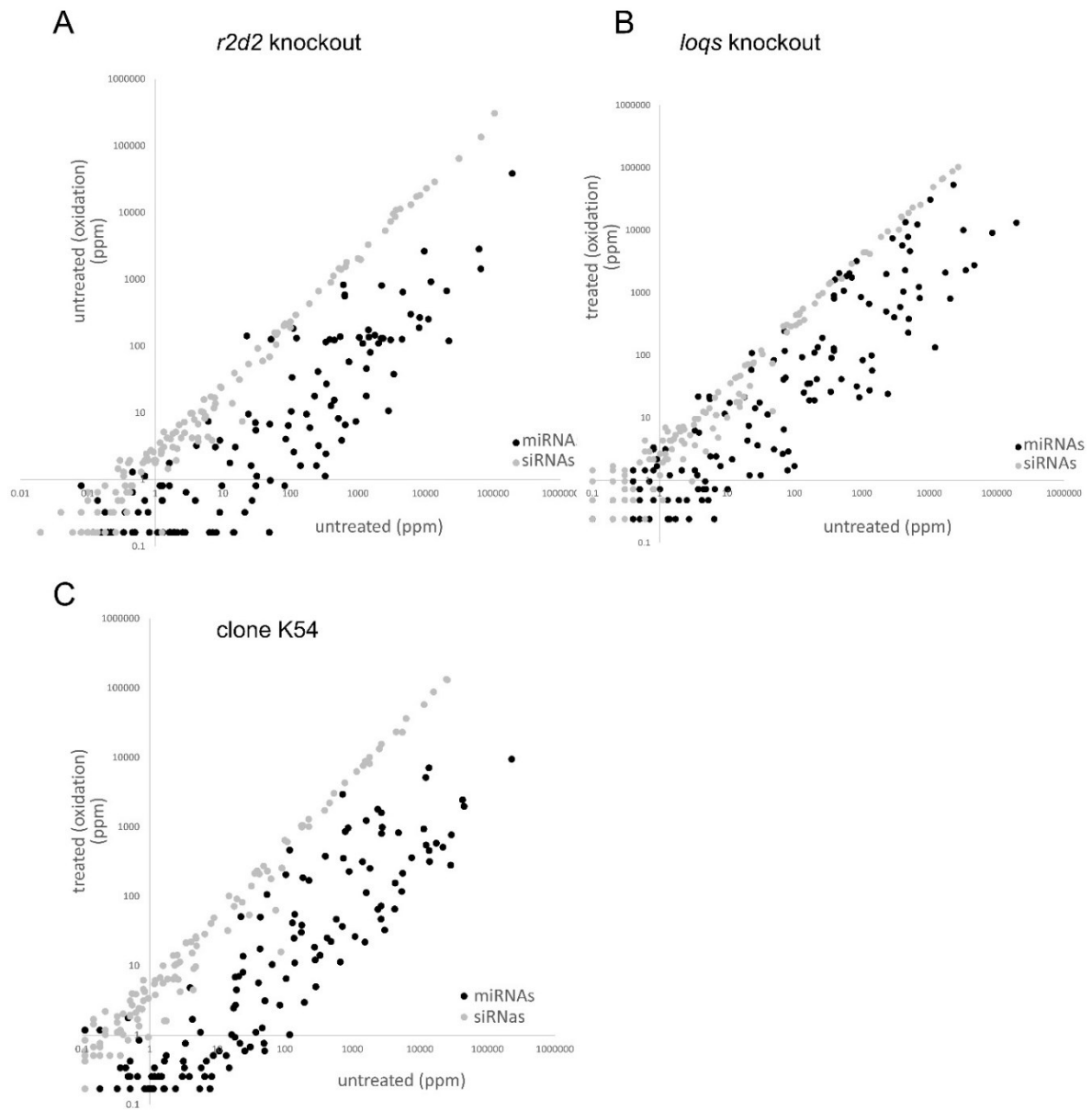
Figure 9. Deep sequencing analysis of small RNA library of treated (oxidation) or untreated cells of single knockout clones. (A) Small RNA profile of *r2d2* knockout cell line with or without oxidation of the RNA. (B) Small RNA profile of *loqs* knockout cell line with or without oxidation of the RNA. Normalized to genome matching reads. (C) Small RNA profile of clone K54 with or without oxidation of the RNA. Normalized to genome matching reads.

To illustrate our hypothesis for changes in the small RNA profile of a true *loqs/r2d2* double knockout cell line, total RNA from induced (10 µM CuSO₄) and uninduced Dcr-2 clone 1 was extracted and either treated with periodate or not. This should show the expected phenotype for the *r2d2* knockout with inducible Loqs-expression (clone K54 uninduced). Figure 10A displays the resulting small RNA profile after deep sequencing of the small RNA libraries. Turning off the expression of Dcr-2 should remove the siRNAs from the system (Figure 10A, red datapoints).

Compared to the induced sample where the Dcr-2 expression is turned on, one can observe a clear shift of the siRNAs compared to uninduced sample where the Dcr-2 expression is turned off (Figure 10A, compare red and black data points). The miRNAs in the uninduced sample (light pink) are also scattered above the diagonal formed by the data points of the siRNAs and not just below. When comparing the abundance of siRNAs in uninduced and induced cells the remaining activity of Dcr-2 is visible because siRNAs are not missing completely. They shifted from the diagonal in the induced sample upon oxidation (Figure 10B). The miRNAs do not show these lateral changes in the graph (Figure 10C). One can detect a slight general trend towards lower abundance after oxidation since the data points are towards the origin along the diagonal. The effect of the induced or uninduced Dcr-2-expression on miRNAs is as strong as on siRNAs since miRNAs are processed by Dcr-1 and should not be affected by a knockdown of Dcr-2. All in all, these results show that when turning off the Dcr-2 expression in the inducible Dcr-2 clone 1 one can still detect some loading of Ago2.
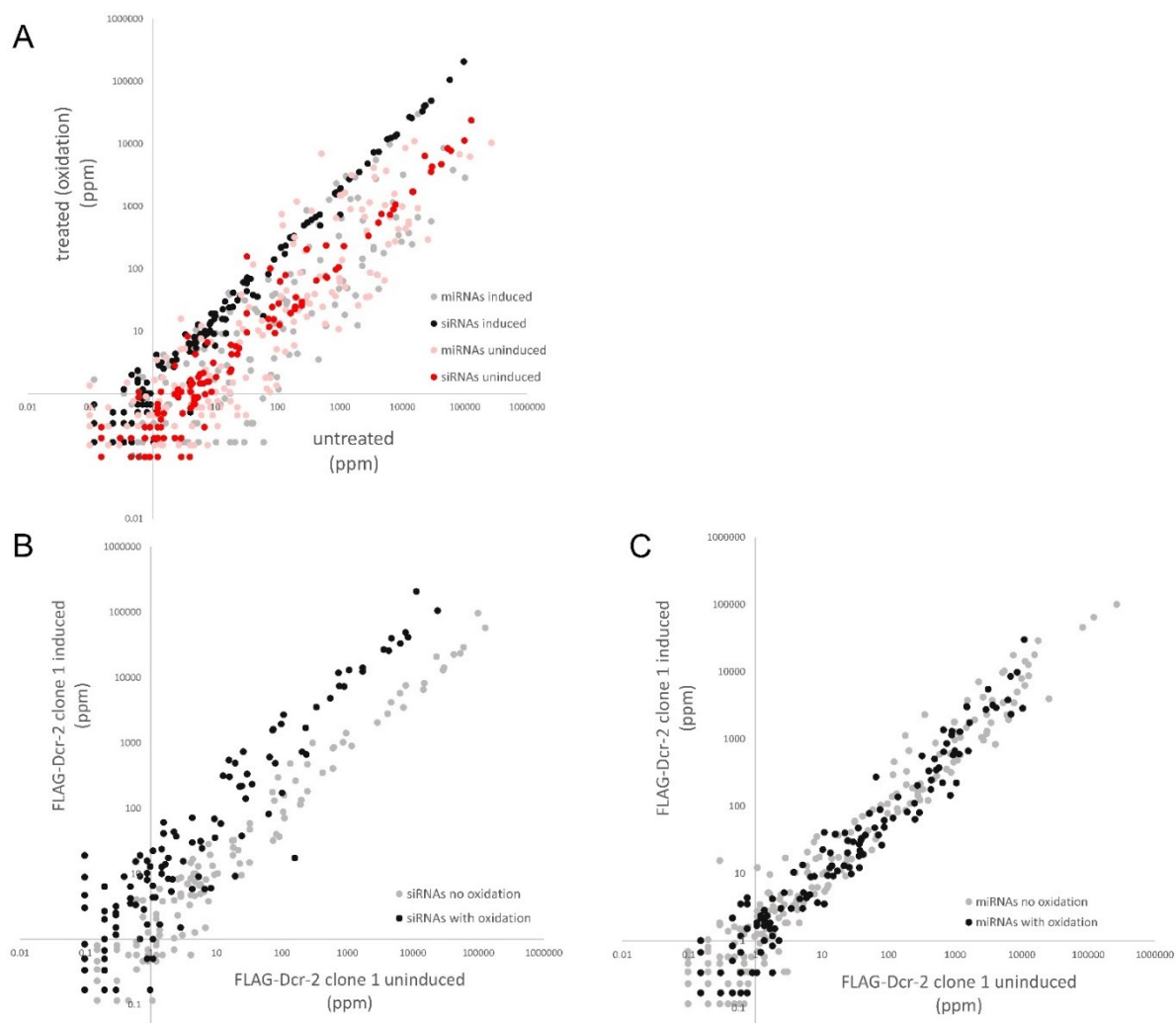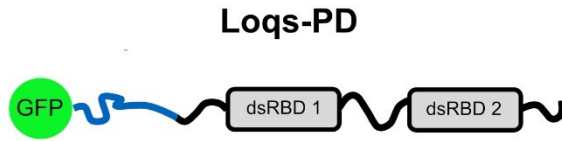
Figure 10. Deep sequencing analysis of small RNA library of FLAG-Dcr-2 clone 1. (A) Comparison of the small RNA profile of treated (oxidation) or untreated RNA of FLAG-Dcr-2 clone 1 cells in the induced vs. uninduced state. (B) Abundance of siRNAs of treated (oxidation) or untreated RNA of FLAG-Dcr-2 clone 1 cells in the induced vs. uninduced state. Normalized to genome matching reads. (C) Abundance of miRNAs of treated (oxidation) or untreated RNA of FLAG-Dcr-2 clone 1 cells in the uninduced vs. induced state.

Analysis of liquid-liquid phase separation with the help of GFP-Loqs-PD fusion proteins

The GFP-Loqs-PD wildtype (wt) construct (Figure 11A) was cloned by PCR and restriction digests of a plasmid backbone (pLT2). The pLT2 plasmid serves as a backbone for all of the GFP-Loqs-PD constructs that were cloned. It includes a monomeric GFP variant and downstream two adjacent restriction digest sites for the endonucleases *KpnI, NotI* and *XbaI*. Like this, every sequence with the analogous restriction sites can be inserted downstream the GFP sequence to generate a N-terminal GFP fusion. Transfection of S2-cells K54 (uninduced) with the GFP-Loqs-PD wt construct

(pSM11) revealed cytoplasmic localization of Loqs-PD and the formation of condensates (Figure 11B). To verify that Loqs-PD is forming condensates in cells and GFP is not driving the condensate formation, a control with only GFP was transfected and examined in cells. GFP only (GFP control, pLT2) did not form condensates in cells (Figure 11B). Upon treatment of transfected cells with 10 % 1,6-hexanediol for one hour, the Loqs-PD condensates dissolved. 1,6-hexanediol inhibits weak hydrophobic protein-protein/protein-RNA interactions. FRAP-assays where entire Loqs-PD wt condensates were bleached demonstrated that they recovered their fluorescence intensity up to approximately 60 % of the initial level within 30 seconds after the bleaching event. By bleaching the entire condensate, it was possible to detect the exchange with the surrounding dilute phase (cytoplasm). Thus, the formation of Loqs-PD wt condensates is reversible by the addition 1,6-hexanediol and bleached condensates are recovering their fluorescence by exchanging molecules with the cytoplasm. These results strongly argue for the liquid-like nature of Loqs-PD wt condensates formed by liquid-liquid phase separation.
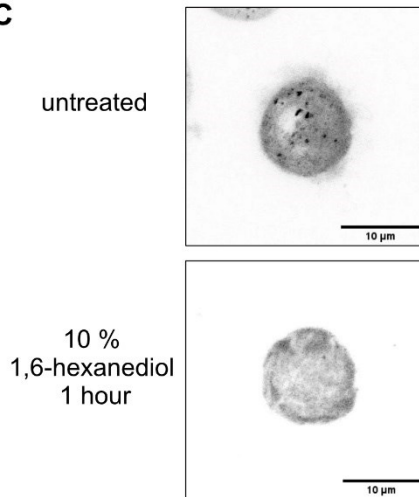
A

Loqs-PD

B

DNA (blue) Loqs-PD (green) composite GFP (control)

C

untreated

10 % 1,6-hexanediol 1 hour

D

pre-bleach 3 sec. 5 sec. 15 sec. 30 sec.
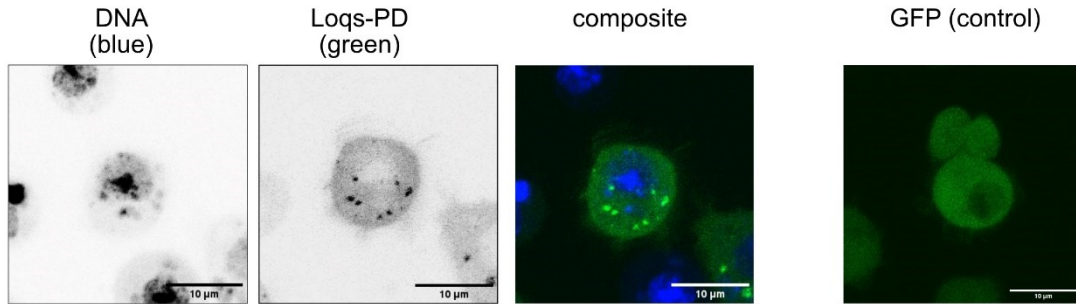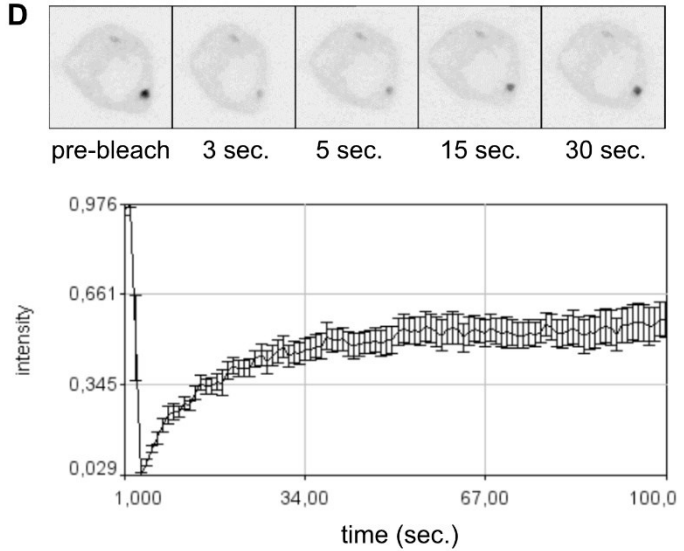
Figure 11. The liquid-like nature of Loqs-PD in S2-cells K54 uninduced. (A) Schematic of GFP-Loqs-PD fusion protein. GFP (green sphere) was fused to the N-terminus (blue) of Loqs-PD. The dsRBDs are displayed as rectangles and are connected by the unstructured linker (black) with the C-terminus at the end (black). (B) Representative confocal microscopy image of live cells with Loqs-PD in green and DNA stained with Hoechst 33342 (blue). Scale bar 10 µM. (C) Representative image of clone K54 (-) transfected with GFP-Loqs-PD untreated and treated with 10% 1,6-hexanediol for 1 hour. Scale bar 10 µM. (D) Upper row: time series of a Loqs-PD condensate during FRAP-assay from before the bleaching up to 30 seconds after the bleaching event. Below: Average recovery curve of the initial fluorescence intensity of 11 Loqs-PD condensates with the standard error plotted as error bars.

Cloning of different Loqs-PD constructs to identify the sequence features for condensate formation

To identify the sequence responsible for the Loqs-PD condensate formation *in vivo*, various Loqs-PD constructs have been cloned and transiently transfected into S2-cells K54 (uninduced) for live cell imaging. Figure 12A shows a scheme of Loqs-PD with highlighted parts of the sequence that have been modified to generate different expression plasmids. To examine the impact of the Q/N-rich N-terminus of Loqs-PD on phase separation behavior, in the first Loqs-PD variant all of the glutamine (Q) and asparagine (N) residues in the N-terminus of the protein have been replaced by alanine (A) (pSM14). The expression of the GFP-Loqs-PD Q/N→A variant led to condensate formation in cells that were of similar size and shape compared to the wt protein but with slightly higher number of condensates per cell (Figure 12B, C). It has been shown that the affinity of the dsRBDs to bind dsRNA relies on two lysines that make critical contact with the dsRNA (Tants et al., 2017). Mutations of the corresponding amino acids in *Drosophila* dsRNA binding protein Blanks, resulted in a 10-fold reduction of the dsRNA binding affinity (Nitschko et al., 2020). A 10-fold reduction of dsRNA binding affinity was also observed with the corresponding mutations introduced in a human protein (NF90) (Schmidt et al., 2016). Therefore, Loqs-PD constructs with the substitution of these two lysines by two alanines (KK→AA) in the dsRBD1 and 2 were cloned to examine the effect of the binding capability of the dsRBDs on condensate formation. To identify whether which of the dsRBDs could be responsible for a possible change in the condensate formation pattern, the KK→AA mutation was introduced in either dsRBD1 or dsRBD2. GFP-Loqs-PD KK→AA dsRBD1 (pSM42) showed condensates in the cells whereas GFP-Loqs-PD KK→AA dsRBD2 (pSM41) showed a clearly reduced number of condensates relative to the wildtype (Figure 12B, C). Combined inactivation of both dsRBDs has the same effect as inactivation of dsRBD2 only. Combining the KK→AA substitutions in both dsRBDs with the Q/N→A mutations (pSM19) showed slightly more condensates than the one with the point mutations in both dsRBDs only (Figure 12B, C), arguing that any effects resulting from a changed IDR sequence content and diminished dsRNA binding capability occur independently of each other. In summary, these results clearly show that the intact dsRBD2 and its ability to bind dsRNA is crucial for the formation of Loqs-PD condensates.
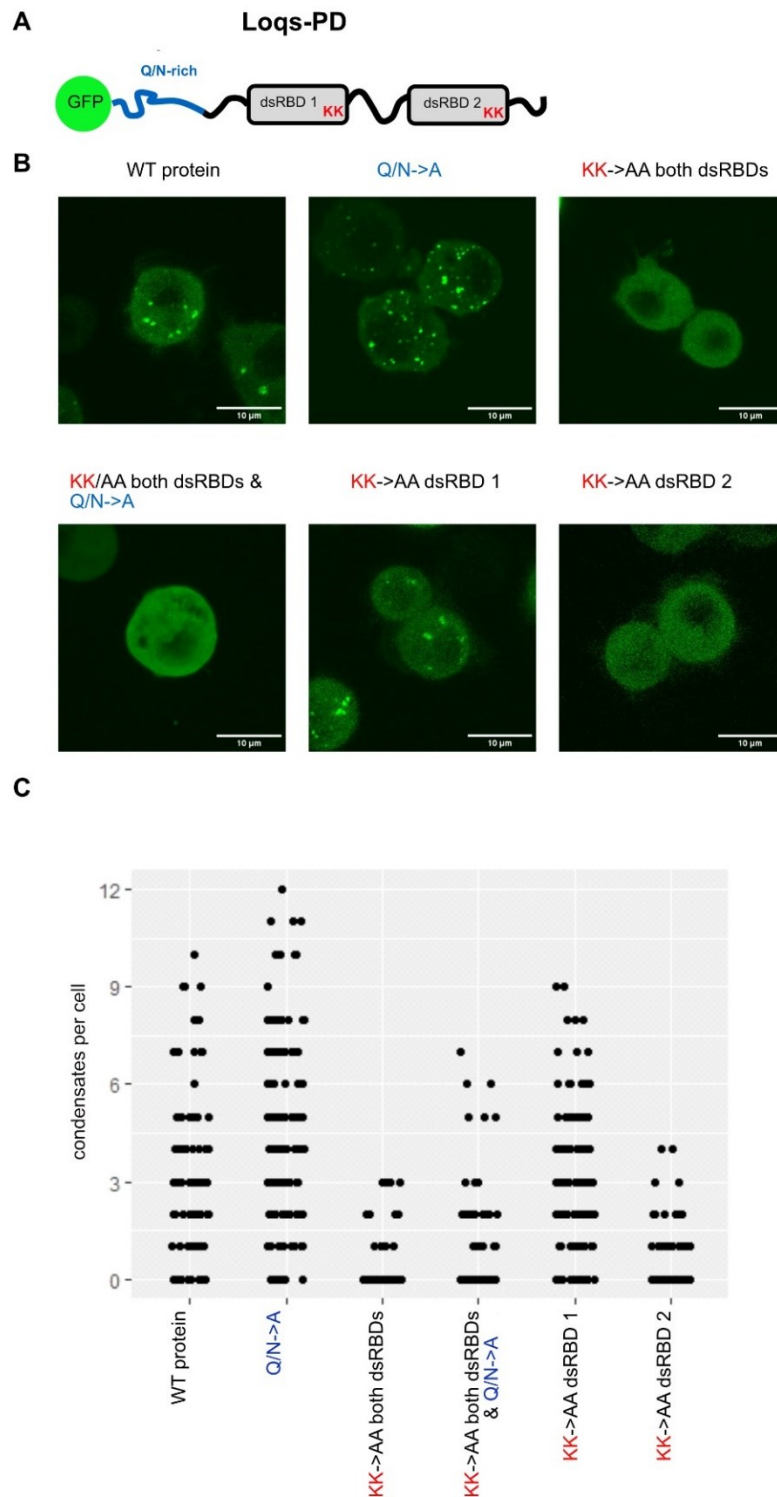
Figure 12. Loqs-PD dsRBD2 is crucial for condensate formation *in vivo*. (A) Schematic of GFP-Loqs-PD fusion protein with indicated sites of modifications. (B) Representative confocal microscopy images of live cells transfected with indicated GFP-Loqs-PD constructs. Scale bar 10 μM. (C) Quantification of condensates per cell of indicated GFP-Loqs-PD constructs. Number of cells analyzed: WT protein: 87; QN→A: 134; KK→AA both dsRBDs & QN→A: 69; KK→AA dsRBD1: 68; KK→AA dsRBD2: 48.

In addition to experiments in live cells, I was able to demonstrate the same effects of the mutations in the sequence of Loqs-PD in ovaries of transgenic fly lines. Figure 13 shows confocal microscopy images of a germarium of the respective fly lines stably expressing the different Loqs-PD-constructs. The germarium is the most apical structure of a fly ovary where the stem cells are located followed by the developing egg chambers, nurse cells and follicle cells (Kirilly & Xie, 2007). As shown in Figure 13, GFP-Loqs-PD wt forms condensates in fly ovaries. When both of the dsRBDs or only dsRBD2 are mutated (KK→AA) a reduced number of condensates was observed. There are some condensates visible at the most apical part of the germarium though in both of the transgenic fly lines with mutations in dsRBD2 (Loqs-PD KK→AA in dsRBD1 and Loqs-PD KK→AA both dsRBDs). When only dsRBD1 is mutated, one can see condensate formation in the germarium. The control (only GFP) shows that in flies stably expressing GFP as well as in cells transiently expressing GFP (Figure 12), there is no condensate formation visible (Figure 13). The transgenic flies expressing only GFP were made by injecting pRB10, a plasmid that contains GFP under control of a ubiquitin promoter (ubi64E) (same promoter as in pLT2). The follicle cells (Figure 13, labeled with a white arrowhead) which surround the egg chambers budding off the germarium do not show any Loqs-PD spots in any of the transgenic fly lines. The transgenic flies expressing GFP only demonstrate that the proteins are nonetheless expressed at similar levels as in the germline. FRAP assay of condensates formed in the germarium of the GFP-Loqs-PD wt-flies were difficult to measure. It was not possible to bleach and monitor the recovery of wild type condensate. As visible in Figure 14 A, the fluorescence intensity of the samples was very low and the maximum laser intensity was needed to capture the images of the fly tissues. The maximum laser intensity led to quick bleaching of the complete tissue. Therefore, it was not possible to bleach a single condensate and at the same time record the recovery of fluorescence since capturing the images after the time of the bleaching event bleached the entire tissue. It was possible to bleach and monitor the recovery of fluorescence of condensates formed in the germarium of fly lines stably expressing GFP-Loqs-PD KK→AA in dsRBD1 (Figure 14B upper row). The average recovery curve (Figure 14B bottom) showed that the bleached condensates did not recover fluorescence during the recorded time after the bleaching event (90 sec.). This result is consistent with the observations made in cells where the condensates formed by GFP-Loqs-PD KK→AA dsRBD1 also did not recover their fluorescence after photobleaching.
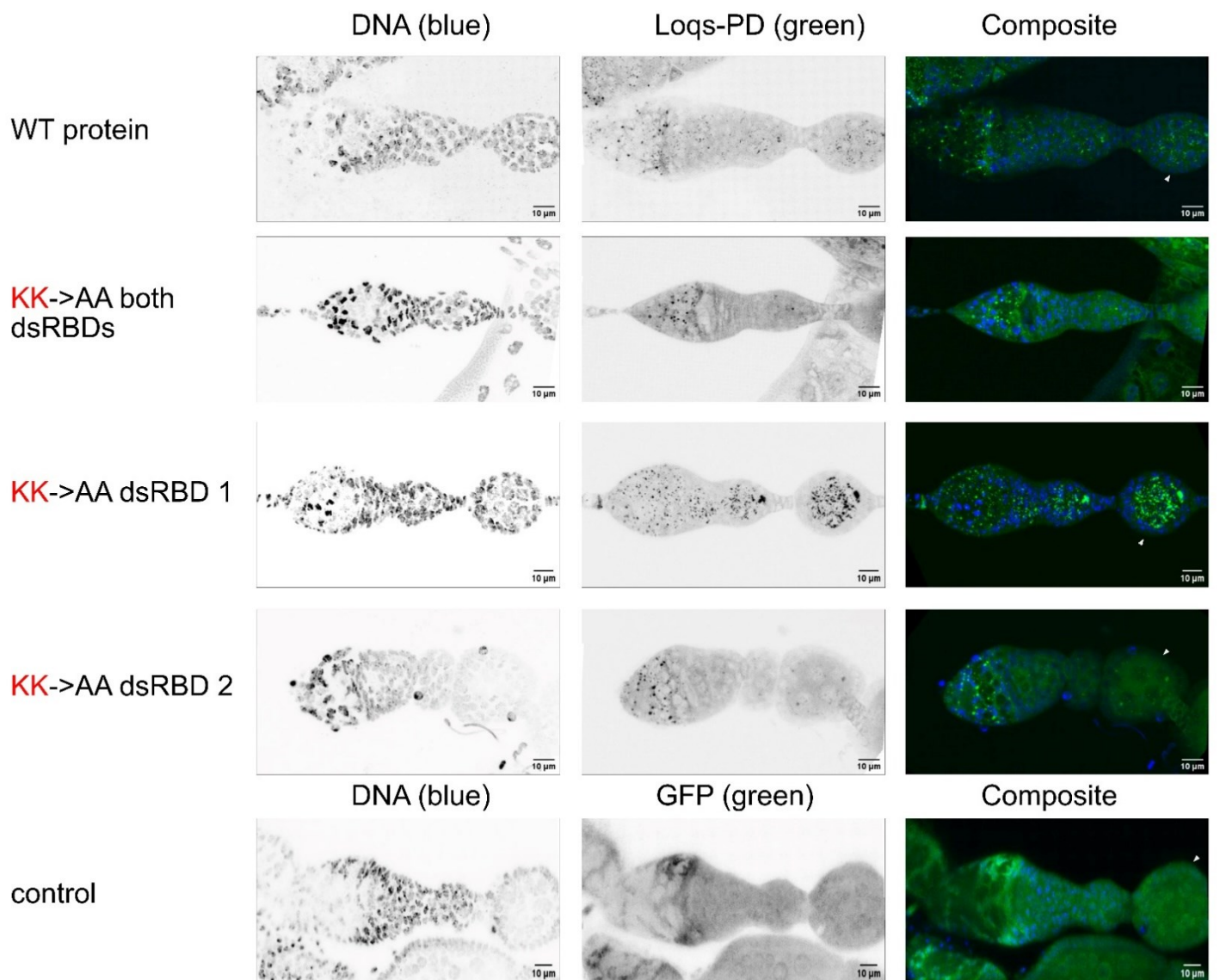
Figure 13. Loqs-PD constructs stably expressed in flies. Representative confocal microscopy pictures of germariums of fly lines stably expressing the indicated GFP-Loqs-PD variants and as a control only a fly line stably expressing GFP. White arrowheads pointing on follicle cells. Scale bar 10 µM.
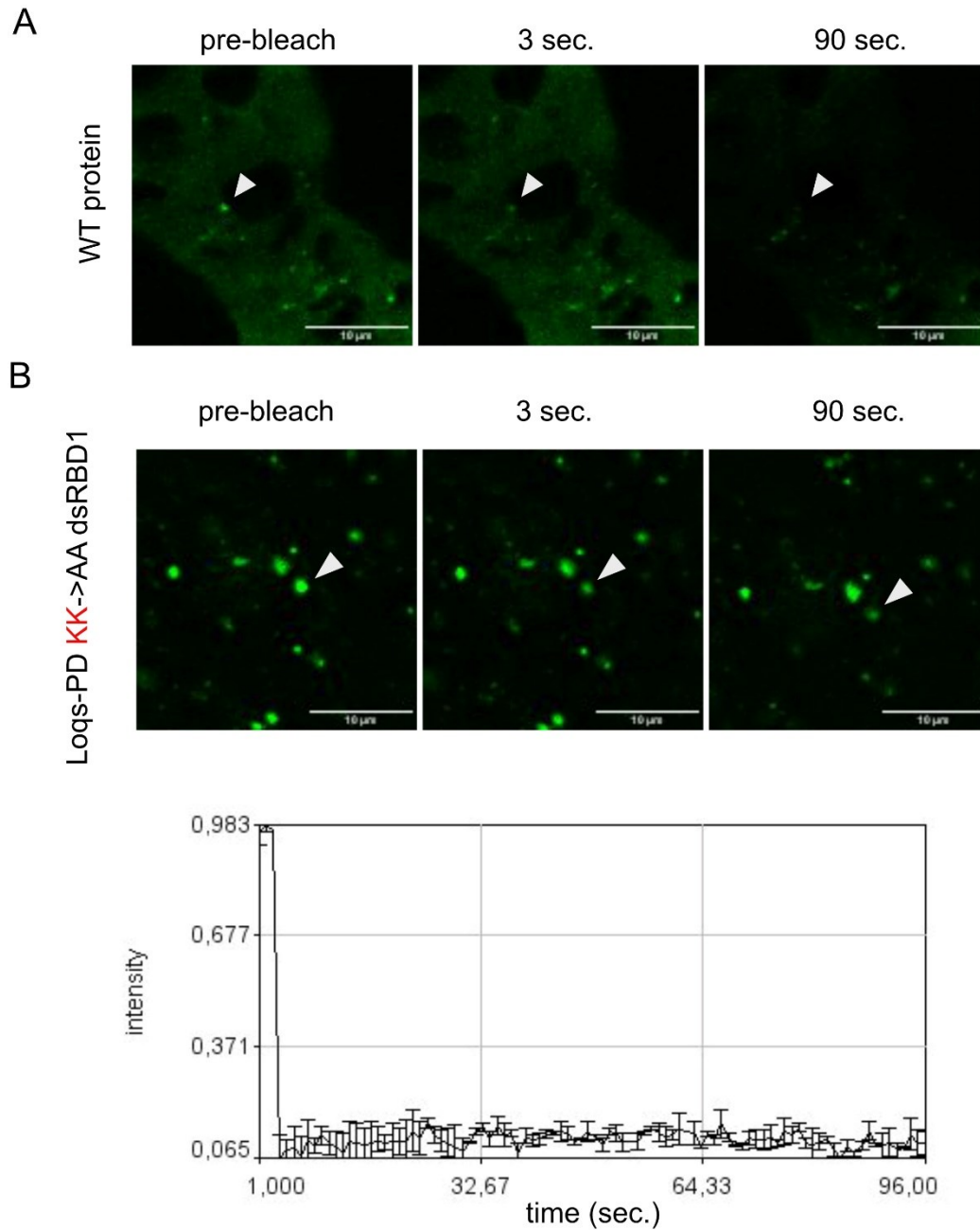
Figure 14. FRAP assay of condensates located in the germarium of fly lines stably expressing GFP-Loqs-PD wt or KK→AA dsRBD1. (A) Image of three different time points (pre-bleach, 3 sec. and 90 sec. after the bleaching event) of a germarium from a fly stably expressing GFP-Loqs-PD wild type. White arrow head points on the bleached condensate. (B) Upper row: image of three different time points (pre-bleach, 3 sec. and 90 sec. after the bleaching event) of a germarium from a fly stably expressing GFP-Loqs-PD KK→AA dsRBD1. White arrow head points on the bleached condensate. Below: Average recovery curve of the initial fluorescence intensity of two Loqs-PD KK→AA dsRBD1- condensates with the standard error plotted as error bars.

2.2 Colocalization of Loqs-PD and Dicer-2

Genomic engineering of S2 cells to generate an inducible Dcr-2 cell line

The same strategy as for clone K54 was applied to generate an inducible Dcr-2 cell line. Via the CRISPR/Cas9 system, an expression cassette with a metallothionine promoter and 3xFLAG-tag was inserted into the genome of 5-3 cells (S2-cells stably expressing Cas9) to replace the endogenous Dcr-2 promoter. The single cell clone resulting from this cell line was called FLAG-Dcr-2 clone 1. To verify the absence of Dcr-2 in clone 1 in the uninduced state, total protein was isolated and separated on a polyacrylamide gel and detected with a mouse monoclonal Dcr-2 antibody (Miyoshi et al., 2009). The western blot shows the inducible Dcr-2 clone 1 with 250 μm $CuSO_4$ and uninduced, as well as wild type cells as a control (Figure 15A). When inducing Dcr-2 with 250 μM $CuSO_4$ we can see a thick band indicating overexpression of the protein in the cells. In extract from wildtype cells, one can see the expression level of endogenous Dcr-2. Previous titration experiments showed that the endogenous expression levels can be reached by adding approximately 150 μM $CuSO_4$ to the medium of FLAG-Dcr-2 clone 1 (Figure 15B). Without the induction of Dcr-2 in the inducible Dcr-2 clone 1, there is no band for Dcr-2 visible on the western blot indicating that with this clone 1 it is possible to achieve a cellular state equivalent to a Dcr-2 knockdown (Figure 15A). The agarose gel in Figure 15B shows the PCR products of isolated genomic DNA of wild type cells and the inducible Dcr-2 clone 1. A PCR product with 200 nt size indicates the wild type allele whereas a PCR product of 650 nt is expected for the tagged *dcr-2* locus. Since there is no band at the size of 200 nt in the case of the inducible Dcr-2 clone 1, one can assume that every *dcr-2*-allele was tagged successfully and no wt-alleles are left (Figure 15C). Sequencing of the PCR product of Dcr-2 clone 1 revealed that part of the HDR cassette that was originally inserted through tagging got lost in the single cell clone. Part of the metallothionine-promoter and the blasticidin resistance is no longer there.
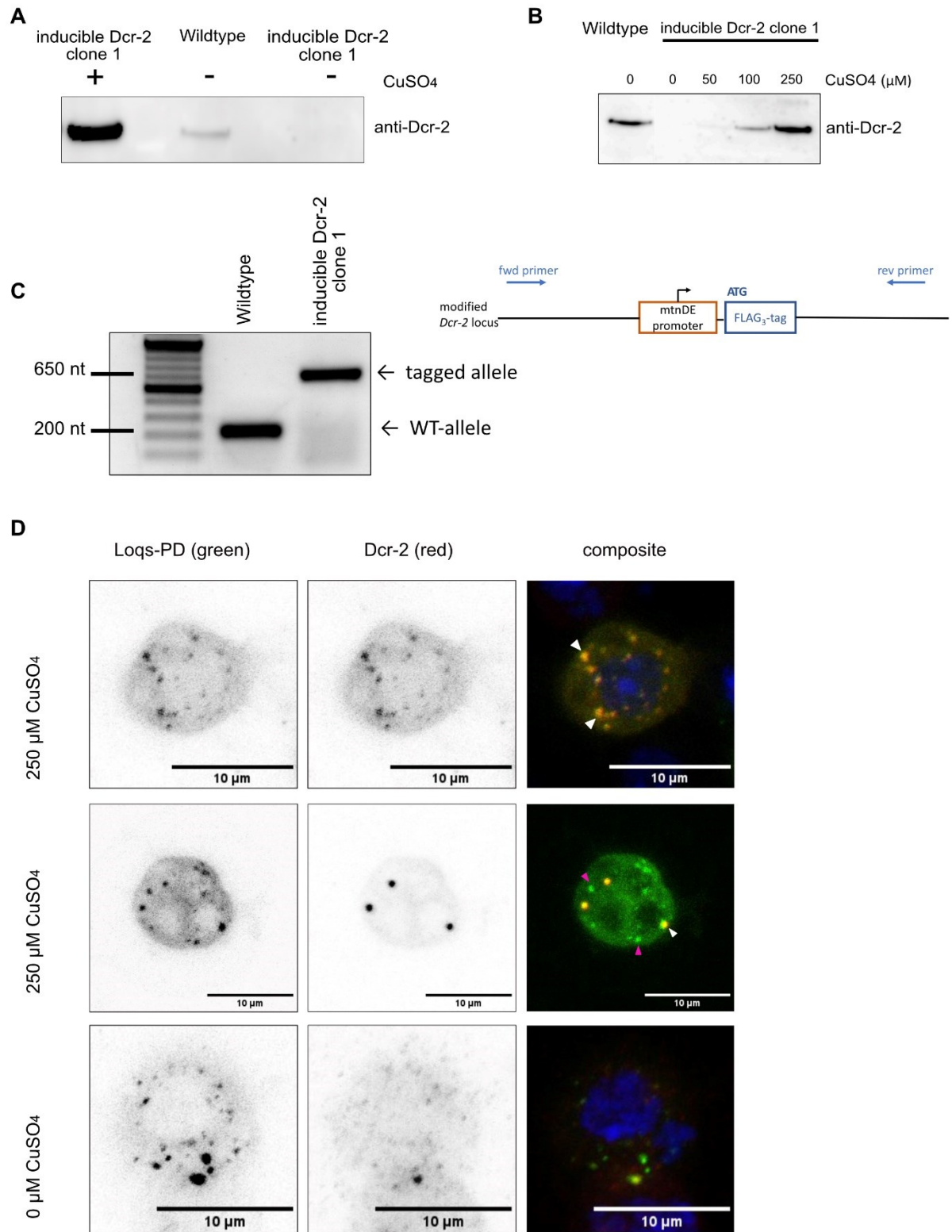
Figure 15. Inducible FLAG-Dcr-2 colocalizes with Loqs-PD. (A) Western blot (anti-Dcr-2) of inducible Dcr-2 clone 1 induced with 250 µM CuSO₄, wild type cells and inducible Dcr-2 clone 1 uninduced. (B) Western blot (anti-Dcr-2) of wildtype and inducible Dcr-2 clone 1 with 0 µM, 50µ M, 100 µM or 250 µM CuSO₄. *Legend continues on following page.*

Figure 15. (C) PCR of genomic DNA of wild type cells and inducible Dcr-2 clone 1 on a 1%-agarose gel and schematic drawing of the modified *Dcr-2* locus with PCR primer binding sites indicated. (D) Representative confocal microscopy images of immunostaining of inducible Dcr-2 clone 1 induced with 250 µM CuSO₄ (upper and middle row) or uninduced (lower row) transfected with GFP-Loqs-PD wt. White arrowheads point to condensates where Loqs-PD and Dcr-2 colocalize. Magenta arrowheads point to Loqs-PD condensates. Scale bar 10 µM.

Colocalization of Loqs-PD and Dicer-2

It has been shown previously that Dcr-2 localizes to cytoplasmic granules called D2-bodies in S2-cells (Nishida et al., 2013). To investigate whether Loqs-PD localizes to the same condensates as Dcr-2, Dcr-2 clone 1 (induced) was transiently transfected with GFP-Loqs-PD and immunostaining of fixed cells was performed. Dcr-2 was stained with a FLAG-antibody (secondary antibody coupled to a red fluorophore Alexa 594™) and Loqs-PD was additionally stained with a GFP-antibody coupled to a green fluorophore (Alexa 488™) to enhance the remaining GFP fluorescence. The immunostaining shows that when co-overexpressing Dcr-2 by inducing it with 250 µM CuSO₄, Dcr-2 forms condensates in cells as well as Loqs-PD (Figure 15D, upper row). The composite shows that the signals for Loqs-PD and Dcr-2 overlap. When the expression of Dcr-2 is not induced, only Loqs-PD condensates are visible in the stained cells. These results suggest that Loqs-PD and Dcr-2 do colocalize to the same condensates in S2 cells and overexpressed Loqs-PD can replace the requirement for R2D2 in D2-body formation.

2.3 Recombinant protein expression of the N-terminus of Ago2 (1-413 aa)

To purify the N-terminus (amino acids 1-413) of Ago2 a new expression plasmid was cloned (pSM2). The Ago2 N-terminal sequence was amplified via PCR from gDNA of the Oregon-R fly lab strain. During the PCR restriction sites for the endonucleases *NdeI* and *EcoRI* were added. The plasmid pKF306 (containing MBP – Strep-tag – His-tag) was used as vector backbone, digested with the same restriction enzymes and finally ligated with the digested PCR product. The resulting plasmid (pSM2) (Figure 16A) was transformed in JM109 competent cells to inoculate medium for a liquid bacterial culture. JM109 are an *E. coli* K12 derivative with a DE3 insertion that contain a chromosomal copy of T7 RNA polymerase for high-level expression of genes cloned downstream the T7 promoter. The expression of the recombinant protein was induced with 1 mM IPTG overnight at 23 °C. The cells were harvested, lysed and purified with Ni-NTA agarose beads at 4 °C (see Materials and Methods). In a second step, the elution fraction from the prior purification was purified again via streptactin superflow beads. Figure 16B

displays the polyacrylamide gel loaded with samples from different purification steps. The purification with Ni-NTA-agarose beads worked reasonably well. However, the subsequent purification of the Ni-elution fraction with streptactin superflow beads resulted in only low yield. The plasmid pSM2 was sent to our collaborators (Sattler lab, Technical University Munich) and served as starting point for cloning of important recombinant protein expression plasmids for *in vitro* experiments of our common project.
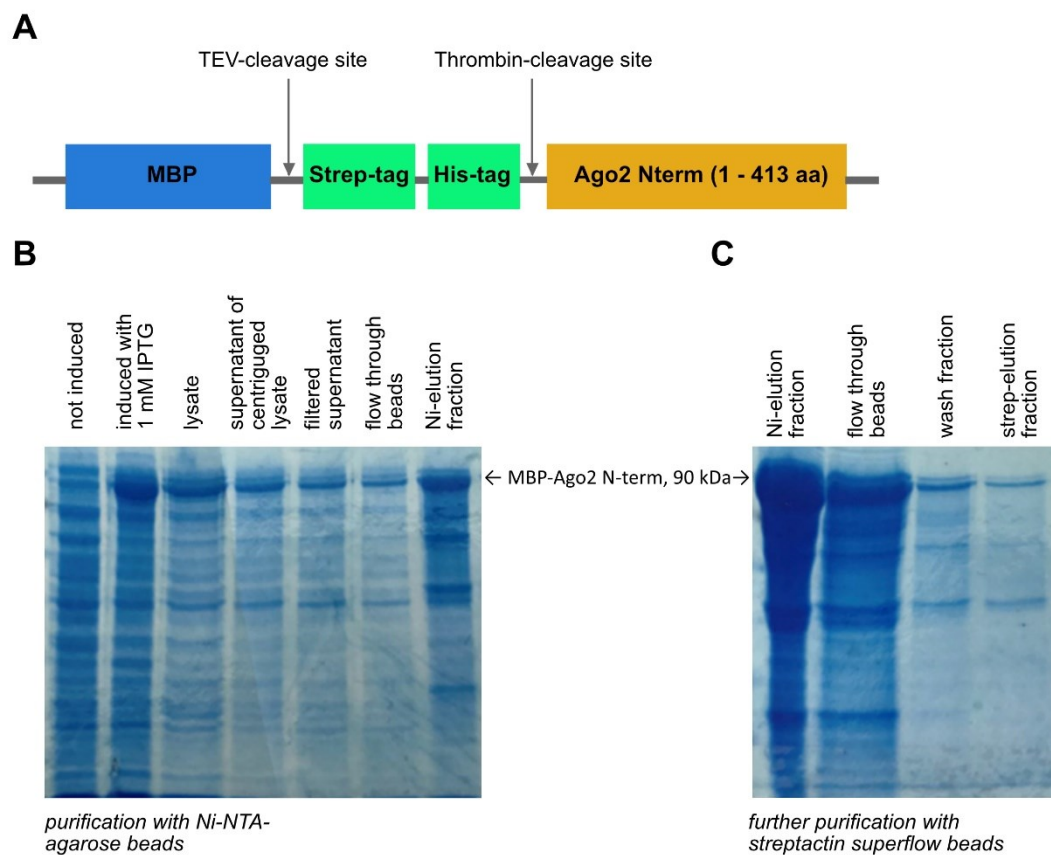
Figure 16. Recombinant expression of Ago2 N-terminus (1-413 aa). (A) Schematic of fusion protein Ago2 N-terminus (1-413 aa) with MBP, TEV-cleavage site, Strep-tag, His-tag, Thrombin-cleavage site. (B) 10 %-polyacrylamide gel of different purification steps of recombinant Ago2 N-terminus with Ni-NTA agarose beads. The following fractions were loaded on the gel: 0.0005 % of the not induced and induced bacterial cell culture, 5 % of the lysate, 5 % of the supernatant of centrifuged lysate, 5% of the filtered supernatant, 5 % of the flow through beads and 0.1 % of Ni-elution fraction. (C) Subsequent purification with streptactin superflow beads. The following fractions were loaded on the gel: 0.45 % of Ni-elution fraction, 22.5 % of the flow through beads, 1.125 % of the wash fraction and 2.25 % of the strep-elution fraction.

2.4 Generation of an Ago2 fusion protein to examine its cellular localization

To investigate the cellular localization of Ago2 and a possible co-localization with Loqs-PD, a tdTomato-Ago2 fusion protein (pRB92) was cloned. When expressing the protein in 5-3 cells, strong proteolysis was visible on the anti-RFP western blot (Figure 17A, left). Most of the fusion protein was degraded in cells and only a small amount of full-length fusion protein remains (193 kDa). There are many degradation products visible on the blot and a very thick band at the size of tdTomato (56 kDa). When examining these cells under the confocal microscope, one can see red fluorescent structures like condensates and fibers in the cell (Figure 17B, upper row). When transfecting only tdTomato (pRB91) as a control the same structures can be found and after seven days they turn into fibers. TdTomato on its own seems to form condensates and fibers and thus cannot be used as a fusion partner for examining the cellular localization of Ago2 since there is no way to distinguish between condensates formed by the tdTomato-Ago2 fusion protein or tdTomato only. Exchanging tdTomato to mCherry to avoid the problem that tdTomato forms condensates on its own did not change the amount of proteolysis in the cells. The mCherry-Ago2 fusion protein (163 kDa; pSM49) was prone to proteolysis as well (Figure 17A, right). The full-length fusion protein is barely visible on the anti-RFP western blot but mCherry (30 kDa) and degradation products are visible. Under the confocal microscope, the cells transfected with the mCherry-Ago2 fusion protein showed some condensates (Figure 17B, bottom row). Since cells transfected with only mCherry (pTG2) showed the same kind of condensates, this construct cannot be used for localization experiments of full-length Ago2. A third approach to fuse GFP to Ago2 also did not lead to the expected results. The GFP-Ago2 fusion protein showed strong proteolysis in cells, too (Figure 17D) as detected on the anti-GFP western blot. The amount of GFP-Ago2 full-length fusion was much lower compared to the amount of GFP only in the same lane. In very few cells, GFP-Ago2 (pTG1) showed some condensates whereas the control with GFP only did not show condensates in cells (Figure 17D). S2-cells that stably express only the Q-rich N-terminus (1-413 aa) of Ago2 fused to GFP (pKF310) formed spots resembling the morphology of condensates (Figure 18A). These condensates seem to exhibit a more solid-like state since they do not recover their fluorescence during FRAP-assays and or did not bleach at all (Figure 18B). Combining the observations during microscopy with the western blot results did not lead to reliable conclusions. It is not certain that condensates of Ago2 fusions with any of the fluorescent proteins used are Ago2 condensates formed by LLPS or condensates that are composed of the respective fluorescent protein only.

The fourth attempt to generate a functioning fluorescent fusion protein was to insert the fluorescent protein (mCherry) after the N-terminus of Ago2 in the middle of the protein sequence. Since the fluorescent protein was cleaved off from the full-length proteins in all three attempts with tdTomato, mCherry and GFP we assumed that a proteolysis sensitive site could be located between the unfolded (N-terminus) and folded part of the protein (Figure 17E). To test this hypothesis, two plasmids were cloned (schematic in Figure 17E) where Ago2 was split into two parts and mCherry was inserted after 413 amino acids (pSM56) or 386 amino acids (pSM58) respectively. On an anti-RFP blot with extracts from cells expressing either one of these constructs the fusion protein was not detectable and only mCherry (30 kDa) or unspecific bands (asterisk) showed up (Figure 17E). There were no condensates detected during microscopy. Taken together, these results demonstrate that it has not been possible to generate a full-length Ago2 N-terminal fusion with any fluorescent protein (tdTomato, mCherry, GFP) tested and also the attempt to integrate a fluorescent protein (mCherry) within the protein sequence to bypass the proteolysis sensitive site inside the N-terminus of the protein did not succeed.

A

tdTomato-Ago2 → 193 kDa

tdTomato → 56 kDa

anti-RFP

←mCherry-Ago2 163 kDa

←mCherry 30 kDa

anti-RFP

B

td-Tomato-Ago2 | tdTomato | tdTomato (7 days p.t.)

mCherry-Ago2 | mCherry

C

GFP-Ago2 → 163 kDa

GFP → 30 kDa

anti-GFP

D

GFP-Ago2 | GFP

E

protease-sensitive site

| mCherry | Ago2 | 1208 aa |

pSM56 | Nterm Ago2 (1) | mCherry (413) | Ago2 (414 – 1208 aa) |

pSM58 | Nterm Ago2 (1) | mCherry (386) | Ago2 (387 – 1208 aa) |

wildtype | pSM56 | mCherry

*

←mCherry 30 kDa

*

anti-RFP

pSM58 | mCherry | wildtype

←mCherry 30 kDa

anti-RFP

Legend on following page.

36

Figure 17. Cloning and expression of Ago2 fusion with fluorescent proteins and localization in cells. (A) Western blots (anti-RFP) to detect tdTomato-Ago2 fusion protein (left) and mCherry-Ago2 fusion protein (right) expressed in 5-3 cells and tdTomato or mCherry only as controls. (B) Representative confocal microscopy pictures of 5-3 cells transfected with tdTomato-Ago2, tdTomato three days and 7 days post transfection, mCherry-Ago2 and mCherry. (C) Western blot to detect GFP-Ago2 in expressed in 5-3 cells and GFP only as control. (D) Representative confocal microscopy pictures of 5-3 cells transfected with GFP-Ago2 or GFP only as control. (E) Schematic of two different mCherry-Ago2 fusion proteins with mCherry in the middle of the protein instead of N-terminal fusion and western blots (anti-RFP) of 5-3 cells transfected with the respective plasmids. Asterisk: unspecific band. Scale bars 10 µM.

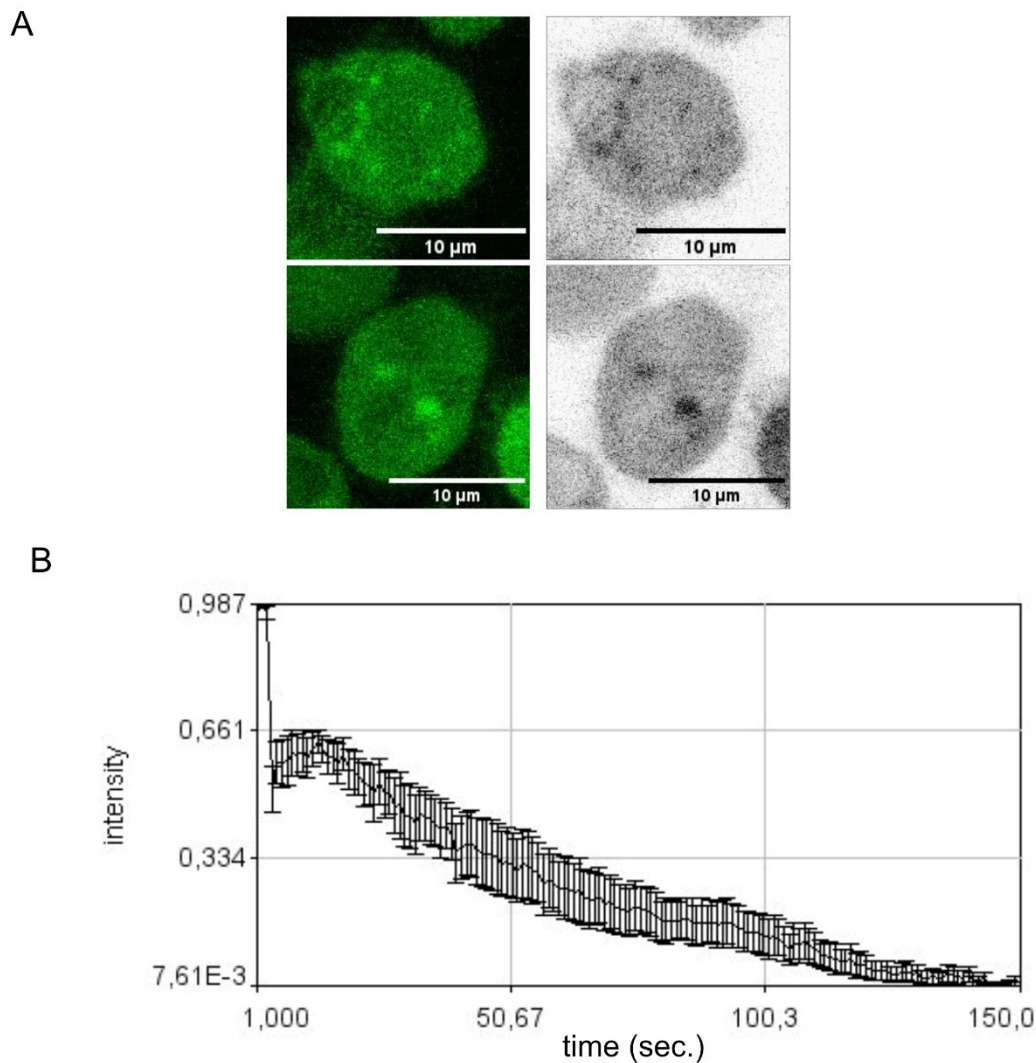**Figure 18. S2-cells stably expressing GFP-Ago2 N-terminus fusion do form condensate-like structures.** (A) Confocal microscopy images in green and black/white of two S2-cells stably expressing GFP-Ago2 N-terminus fusion protein. The cells form condensate-like structures. Scale bar 10 µM. (B) Average recovery curve of the initial fluorescence intensity of 8 condensates with the standard error plotted as error bars.

3 Discussion

3.1 Loqs-PD forms liquid-like condensates dependent on its dsRNA binding capability and colocalizes with Dcr-2

In the present thesis, it has been shown that the D-isoform of Loqs forms condensates in cultured cells via LLPS comparable to the D2-bodies described for R2D2 (Nishida et al., 2013). The two proteins may therefore be redundant in many aspects of their function. Loqs-PD condensates dissolve when 1,6-hexanediol is added to the medium of cultured *Drosophila* cells. 1,6-hexanediol is an aliphatic alcohol that interferes with weak hydrophobic interactions and that is commonly used to dissolve protein condensates to illustrate the reversible character of phase separation (Duster et al., 2021). The fact that Loqs-PD condensates dissolve when the cells are treated with 1,6-hexanediol shows that the condensate formation is reversible. Furthermore, during FRAP-assays bleached Loqs-PD wild type condensates recover their fluorescence intensity during approximately 30 seconds up to 50-60 % of the initial intensity. FRAP is widely used to examine the material properties of condensates and a fast fluorescence signal recovery points to highly dynamic exchange with the surroundings and to a high diffusion coefficient (Taylor et al., 2019). In the case of the observed Loqs-PD condensates, the exchange happens with the surrounding dilute phase, the cytoplasm. The result thus suggests a partially liquid-like nature of Loqs-PD spots. The less mobile or immobile fraction of the Loqs-PD condensate could represent a transition from a liquid- to solid-like state. To further examine the structures that compose the immobile fraction of the Loqs-PD condensates, methods like electron microscopy, X-ray-diffraction or NMR can be used. It has been shown that the properties of a condensate can change over time. The multi-domain RNA-binding protein FUS (full length) is known to phase separate into spherical droplets with initial liquid-like properties and they are progressing to a more solid-like or hydrogel state over time (Burke et al., 2015; Guo & Shorter, 2015). Electron microscopic and X-ray diffraction studies of hydrogel condensates formed by the low-complexity domain of FUS showed that these hydrogels are composed of uniformly polymerized amyloid-like fibers (Kato et al., 2012). Nuclear magnetic resonance (NMR) studies of Nsp1 hydrogels in yeast (ortholog of *Drosophila* Nup62, an essential component of the nuclear pore complex) revealed the evidence of β-structure that can favor the organization into some sort of fibrous network (Ader et al., 2010). The mammalian and fly orthologs of Nsp1p/Nup98 were also precipitated by biotinylated isoxazole microcrystals (Kato et al., 2012).

Biotinylated isoxazole (b-isox in the following) can induce the formation of a precipitate with RNA-granule like composition in cell extracts. This may be linked to the fostering of beta interactions reminiscent of pathogenic amyloid-like fibers. The results for the b-isox assay conducted in the Förstemann lab (unpublished data) with cell extracts of clone K54 transfected with either GFP-Loqs-PD wt, GFP-Loqs-PD dsRBD1 KK→AA or GFP-Loqs-PD dsRBD2 KK→AA correlate with the observations made *in vivo*. Anti-GFP western blots with the respective b-isox treated cell lysates showed a signal in the precipitate for the wt- and dsRBD1 KK→AA-construct but not for the dsRBD2 KK→AA-construct. According to these results, the treatment with b-isox does not induce the formation of a precipitate with RNA-granule like composition when the dsRBD2 of Loqs-PD cannot bind dsRNA.

In vitro experiments can help to examine the requirements for the formation of condensates through LLPS and their and properties more detailed. The *in vitro* work by our project collaborators (Sattler lab, Technical University Munich) supports the *in vivo* observations on condensate formation of Loqs-PD (manuscript in preparation). *In* vitro, the purified untagged Loqs-PD protein as well as GFP-tagged Loqs-PD form condensates that were observed during phase contrast and fluorescence microscopy. Phase separation was induced by the addition of dsRNA. The Loqs-PD construct with KK→AA substitutions in dsRBD2 did not phase separate *in vitro*. The condensates formed by GFP-Loqs-PD wildtype (dsRNA added) were examined during FRAP where a small region inside the condensate was bleached. A partial recovery of the region of interest was observed after approximately 150 seconds after the bleaching event which was considered to be rather slow e.g. due to high viscosity inside the condensate. The *in vitro* results support the observations made *in vivo* that the dsRNA binding capability of Loqs-PD is essential for the formation of condensates and that they exhibit an at least partially liquid-like nature. The co-localization of Loqs-PD with the N-terminus of Ago2 (1-413 aa) and dsRNA has been shown *in vitro*. Interestingly, when the Loqs-PD dsRBD2 was mutated and thus the RNA binding impaired, Loqs-PD did not enter the condensates formed by Ago2 but stayed at the surface. Loqs-PD only enters the condensates formed by Ago2 in the presence of dsRNA when the RNA binding is not perturbed. Therefore, the *in vitro* results propose that dsRNA binding is essential for the formation of coacervates of Loqs-PD with Ago2.

Moreover, I found that dsRBD2 was particularly important for the formation of condensates and that both dsRBDs have to be binding competent to achieve the partially liquid-like state. This argues that the condensates do not only contain protein but most likely also some form of dsRNA. All of the Loqs-PD constructs (both dsRBDs KK→AA, both dsRBDs KK→AA & Q/N→A,

dsRBD2 KK→AA) with mutations in the dsRBD2 form less condensates in cells compared to the wild type construct. Clone K54, which was the cell line transfected for this analysis, still expresses a small amount of functional endogenous Loqs-PD. One could speculate that the remaining endogenous Loqs-PD could build "bridges" to the GFP-Loqs-PD dsRBD2 KK→AA fusion protein and hence some residual spots can still be observed.

Previous studies have shown that proteins with multiple dsRBDs can bind to dsRNA dynamically. That implies that the two dsRBDs can bind independently and the protein might even move along the dsRNA (Koh et al., 2013; Tants et al., 2017; Wang et al., 2015). This assumption is consistent with the idea that dsRBDs may function as "stickers" that form condensates with their multivalent dsRNA. The two dsRBDs are connected by a 45-residue non-structured flexible linker (Tants et al., 2017) that could function as a "spacer". To examine the role of the linker on phase separation, one could generate GFP-fusion proteins with a linker deletion (Δlinker) or shortened linker lengths (short linker) and examine the effect on the condensate formation in cells. In case the GFP-Loqs-PD Δlinker- or GFP-Loqs-PD short linker-construct still form condensates in cells, one could compare the number of condensates with the wildtype and assess whether there are more or less compared to GFP-Loqs-PD wt. FRAP assays to investigate the material properties of possibly forming condensates would be interesting as well. The analysis of potential interactions of the dsRBDs of purified protein with various linker lengths (deletion of 11 up to 41 residues out of 45 residues) by comparing NMR chemical shifts in ^{1}H, ^{15}N correlation spectra showed that the protein-RNA binding interface is not much affected by shortening of the linker (Tants et al., 2017). This is perfectly consistent with their role as "spacer". The NMR-results suggested that a gradual shortening of the linker lead to more pronounced sliding of the protein on the dsRNA ligand. A protein with a shortened linker cannot adopt a domain arrangement required for optimal RNA contacts of both dsRBDs. Consistent with the NMR-results, fluorescence anisotropy experiments showed that the binding affinity for dsRNA of a 41-residue-deletion of the linker sequence exhibits a two-fold reduction compared to the wild type linker. SAXS experiments showed that shortening of the linker restricts the spatial separation of the two dsRBDs. The authors concluded from their experiments that the inter-domain linker enables simultaneous tandem-dsRBD binding of Loqs-PD. Interestingly, the interaction of Loqs-PD with Dcr-2 was not affected by a shortened linker sequence (Tants et al., 2017). *In vivo*, GFP-Loqs-PD-fusion proteins with truncations or deletion of the linker could show whether condensate formation is dependent on the linker since truncation of the linker by 41 residues has been shown to reduce the binding affinity for dsRNA *in vitro*.

The constructs with binding competent dsRBD2 (wildtype, Q/N→A, dsRBD1 KK→AA) do form condensates (Figure 12). These observations made in cells have been validated in flies. In the germarium of transgenic fly lines expressing GFP-Loqs-PD wild type and GFP-Loqs-PD dsRBD1 KK→AA condensates have been observed, too. Whereas in the germarium of flies expressing GFP-Loqs-PD dsRBD2 KK→AA no condensates have been observed (Figure 13). Condensates formed by the GFP-Loqs-PD dsRBD1 KK→AA did not recover after photobleaching in the germarium of transgenic flies (Figure 14). The transgenic flies stably expressing the different GFP-Loqs-PD constructs can be used to demonstrate the functionality of the respective fusion protein by crossing them into the mutant background (*loqs*-ko fly strain) and thus reverting the phenotype in case they are functional. The generation of a double-knock out of *loqs* and *r2d2* or an inducible Loqs in r2d2mutant background in cells was not successful yet but one could also aim for a double-mutant fly. There is a *r2d2* ko fly strain available in the Förstemann lab as well as a *loqs* ko fly strain with a transgene included to restore the expression of Loqs-PB to avoid an impaired miRNA biogenesis. The generation of a *loqs/r2d2* double mutant chromosome via homologous recombination with these fly strains might be difficult since the genes are located on the same chromosome arm (2L) and in close proximity. This attempt would probably involve a lot of screening for the desired progeny and crossings to obtain a fly that is homozygous for the double knockout. It is not impossible though and if successful (viable and fertile flies), one could use the double knockout fly strain e.g. extract RNA for small RNA profile analysis via deep sequencing like it was initially planned for the clone K54 cell line.

The condensate formation of Loqs-PD in the transgenic flies also seems to differ between tissues. In the germline (stem cells and egg chambers) one can observe Loqs-PD condensates whereas in the somatic cells (follicle cells) the protein is expressed but not forming condensates. In case the formation of condensates indicates enhanced Loqs-PD activity here, one could assume that the protein is more active in germline cells of early developmental stages where it might repress transposable elements to secure correct genetic development of the egg. This enhanced activity might be downregulated again in somatic cells because only "basic" activity is needed here. To find out whether Loqs-PD condensates form in other somatic cells or only in the germ line, one could dissect other fly tissues and examine them for possible condensate formation of Loqs-PD. Moreover, fly testes could be dissected and investigated whether one can make the same observations of a difference in condensate formation between germ cells and somatic cells during spermatogenesis as well.

Recently published structures of *Drosophila* Dicer proteins together with dsRBD co-factors confirmed that when the complex does not bind to a dsRNA substrate the dsRBDs are flexible and thus not resolved (Jouravleva et al., 2022; Yamaguchi et al., 2022) . With immunostaining, it was possible to demonstrate the colocalization of Dcr-2 and Loqs-PD in fixed cells of the inducible Dcr-2 clone 1 cell line (Figure 15). It is conceivable that as a first step towards processing the dsRBD co-factors generate condensates with suitable substrate RNAs while they are in complex with their Dicer partners. The colocalization of Loqs-PD and Dcr-2 could increase the efficiency and/or specificity of substrate processing. Immunostaining of the uninduced Dcr-2 clone 1 transfected with GFP-Loqs-PD showed that Loqs-PD can form condensates in absence of Dcr-2 (Figure 15) thus Dcr-2 seems to be dispensable for the condensate formation of Loqs-PD. The observation that overexpression of Loqs-PD leads to condensate formation also in absence of Dcr-2, is consistent with the analysis of the Loqs-PD-paralog R2D2 regarding D2-body formation of Dcr-2 and R2D2. Previous studies (Nishida et al., 2013) showed that Dcr-2 depleted *Drosophila*-cells (depletion through RNAi for Dcr-2) that overexpress R2D2 accumulate R2D2 in cytoplasmic foci similar to D2-bodies. When R2D2 was not overexpressed, Dcr-2 RNAi downregulated not only Dcr-2 but also R2D2 and the D2-bodies disappeared. They concluded that Dcr-2 and R2D2 are both necessary for D2-body formation in distinct ways: Dcr-2 stabilizes R2D2 whereas R2D2 localizes Dcr-2 to the D2-bodies. Overexpression of R2D2 restored spot formation similar to D2-bodies in Dcr-2 depleted cells hence R2D2 is likely critical for D2-body formation (Nishida et al., 2013). To examine whether Loqs-PD only forms condensates whilst overexpressed like it is the case for R2D2, one should repeat the immunostaining in uninduced Dcr-2 clone 1 and do co-immunostaining for Dcr-2 and endogenous Loqs-PD with a Loqs-PD specific antibody. Like this, one can investigate whether endogenous Loqs-PD levels are sufficient for condensate formation in absence of Dcr-2 or whether this condensate formation happens only due to Loqs-PD overexpression. The depletion of Loqs-PD did not affect the appearance of D2-bodies (Nishida et al., 2013). When myc-Loqs-PD was expressed as a transgene, it also did not specifically colocalize to D2-bodies (Miyoshi et al., 2010). Thus, Loqs-PD is dispensable for D2-body formation and does not seem to be essential for the formation of D2-bodies, unlike R2D2 (Nishida et al., 2013). The co-localization of Dcr-2 and Loqs-PD demonstrated in the present work, suggests that Loqs-PD is able to replace R2D2 in the inducible Dcr-2 clone 1 – cell line for the formation of condensates. This result supports the hypothesis that Dcr-2/Loqs-PD can form an alternative RLC and one can further hypothesize that it is spatially separated from the Dcr-2/R2D2-RLC through the localization to different condensates.

The initial plan to generate a *loqs* and *r2d2* double knockout cell line was difficult and at the end not successful in my hands. We wanted to use a *loqs/r2d2* knockout for complementation assays with different *loqs*-variants. Since the generation of a genomically engineered *loqs/r2d2* double knockout has not been successful in the past, I tried to generate an inducible Loqs cell line in the background of an existing R2D2 knockout cell line (Tants et al., 2017). PCR of genomic DNA indicated that not all of the *loqs*-alleles have been modified and additionally, there was a light band visible on the western blot at the size of one of the Loqs isoforms (clone K54, Figure 6). Thus, the genomic editing of all of the *loqs*-alleles was not successful and this led to remaining endogenous protein expression. Two independent tagging-attempts were made. One out of 20 single cell clones from the fist tagging round did not show a signal for Loqs on an anti-Loqs western blot when uninduced. However, PCR of the gDNA of this single cell clone showed a band at the size of the wt-allele. The sequencing results revealed that this clone had a mutation so that the antibody did not bind correctly and therefore there was no signal on the western blot. That's why a second tagging round was made. Here, 72 clones were picked and tested for wt-alleles in a PCR of the gDNA. Two of them did not show wt-alleles in the PCR and were tested for Loqs-expression in the induced and uninduced state with a western blot. One of them was clone K54. Strong growth defects due to the double knock-out situation were not observed, the cells proliferated only slightly slower. When the cells were cultured with $CuSO_4$ they proliferated like wt S2-cells (data not shown). Clonal selection did not seem to be a major problem since there were many clones that were picked and tested. I would suggest to start a new tagging attempt and screen as many single cell clones as possible for wt-alleles and the expression level of Loqs when the cells are not induced until one finds the single cell clone without any wt-allele. The deep sequencing data and qPCR results did not show significant differences between the clone 54 in the uninduced versus induced state or compared to wildtype cells. Therefore, clone K54 was not suitable for experiments like the generation of small RNA libraries with Loqs-PD variants transfected into the double knockdown to examine the effect of mutations in the Loqs sequence on the loading efficiency of Ago2 (Figure 9). We decided to use it for live cell imaging nevertheless because it was the closest that we could get towards a *loqs/r2d2* double knockout. However, the inducible Dcr-2 clone 1 showed the expected phenotype for the Dcr-2 knockdown and the phenotype that has been expected for a *loqs/r2d2* double knockout, too. The number of siRNAs was reduced in cells where the expression of Dcr-2 has been switched off and the miRNAs were scattered above the diagonal formed by siRNAs (Figure 10). Without Dcr-2 expression, the number of siRNAs should decrease because there is no protein processing dsRNA

into siRNAs and thus there are no siRNAs loaded into Ago2. It would have been interesting to examine to localization of Ago2 when Dcr-2 expression is switched off. Unfortunately, we could not examine the Ago2 localization in this context due to the lack of an Ago2 fusion protein. One can find some remaining siRNAs but the difference to the induced sample where the Dcr-2 expression is switched on is clearly visible by the shift of the diagonal formed by the remaining siRNAs towards the x-axis. We normalized the deep sequencing reads from the small RNA libraries to genome matching reads. A synthetic spike-in control or from a foreign species i.e. *Arabidopsis thaliana* could be used for more effective data normalization in the future.

3.2 Attempts to examine Ago2 localization

An important question is the localization pattern of Ago2 and its relation to the Loqs-PD droplets. The highly repetitive N-terminal domain of Ago2 renders both cloning and genome editing challenging. The N-terminal fusions with all of the three fluorescent proteins (tdTomato, mCherry, GFP) were prone to proteolysis, producing a substantial amount of the free reporter protein detectable during live cell imaging and hence preventing reliable imaging of the Ago2 fusion protein (Figure 17). Importantly, only the N-terminus should be used for fusions since the C-terminus, including the terminal COO^- group, plays an important structural role in Ago proteins (Schirle & MacRae, 2012). The expression of a fusion protein with mCherry inserted between the N-terminal IDR and the folded portion of Ago2 did not lead to detectable expression in S2-cells (Figure 17). It has been observed that the depletion of the Ago2 N-terminal domain leaves an Ago2 protein (aa 414-1208) that does not seem to produce condensates. In cell lines stably expressing GFP fused to the N-terminal domain of Ago2, one can observe the formation of condensate-like structures, yet these seem to be more solid-like (Figure 17D). For drawing the conclusion that the N-terminus seems to be important for the formation of condensates *in vivo* from these observations, a comparison with the full-length protein is absolutely essential. The *in vitro* data clearly indicates phase separation of the N-terminal domain of Ago2 (1-413 aa) which is very much enhanced by the addition of nucleic acids (manuscript in preparation).

Attempts to stain endogenous Ago2 in fixed cells via immunostaining have not been successful with the polyclonal and monoclonal antibodies available in the lab. I have tested formaldehyde fixation durations from three to ten minutes with no significant differences between the fixation times. The use of different dilutions (1:100 – 1:1000) of the Ago2-QGQ polyclonal primary antibody or the Ago2-9D6 primary monoclonal antibody in combination with different dilutions of the secondary antibody (coupled to Alexa488™ green fluorophore) did not show a specific

signal in the microscopy images. The cells were just stained green and exhibited some granular structure. To rule out that the observed signal comes from the secondary antibody, the cells were incubated without the primary antibody, the secondary antibody only. These never showed signal during microscopy thus there was no background signal from the secondary antibody that would have disturbed the observation of endogenous Ago2. It seems that the two Ago2 antibodies used here did not bind properly to the protein during the staining process of the fixed cells and thus the signal was not strong enough to be detected during fluorescence microscopy. Defects of the antibodies themselves can be ruled out though since they are binding to protein on western blots. Considering all of the unsuccessful attempts made in the present work, unfortunately, it is still necessary to find a possibility to visualize full length Ago2 *in vivo* to examine where Ago2 localizes relative to the condensates formed by Loqs-PD in cells and in flies. First of all, it would be necessary to show whether Ago2 is actually part of a condensate and whether it is formed by Loqs-PD. This could be achieved with an Ago2 fusion protein that is not prone to proteolysis and in a different color than green. Like this the Ago2 fusion protein and Loqs-PD could be co-expressed in cells and their localization could be examined via live cell imaging. In case the Ago2 fusion protein will not be generated in the future as well, one could improve the immunostaining attempts that were made and try to stain for the endogenous Ago2 while transfecting GFP-Loqs-PD and aim for co-immunostaining. Another possibility would be an inducible Ago2 cell line like it has been generated for Dcr-2. By replacing the endogenous Ago2 promoter with the HDR cassette containing a FLAG-tag, one could use a cell line derived from a single cell clone transfected with GFP-Loqs-PD for immunostaining. Ago2-expression, induce Ago2-expression and stain for Ago2 with anti-FLAG and the anti-GFP to enhance the signal for Loqs-PD (same procedure as for immunostaining of the inducible Dcr-2 clone 1 transfected with GFP-Loqs-PD).

To decipher the functional separation of the small RNA pathways, one could do colocalization experiments with fluorescently tagged Ago1, Loqs-PB from the miRNA pathway and Ago2 and Loqs-PD from the siRNA pathway to examine cross-pathway co-localization. For instance, GFP-Loqs-PD could be co-transfected with an Ago1-fusion protein with a different fluorescent protein than GFP and one could observe whether they colocalize or not during live cell imaging. It can also be done in fixed cells, if e.g. endogenous Ago1 would be stained red and GFP-Loqs-PD is transiently transfected into these cells. Like this one could examine all of the combinations of these four proteins when they are tagged with different fluorescent labels and investigate whether Loqs-PD and Ago2 from the siRNA-pathway are forming condensates that are distinct

form condensates formed by Loqs-PB and Ago1 from the miRNA-pathway and thus the formation of condensates through LLPS it a way to achieve functional separation of these two pathways in *Drosophila*.

3.3 Conclusion and outlook

In the present work, I demonstrated that Loqs-PD forms condensates in *D. melanogaster* cells and flies dependent on the binding capability of the dsRBD2 of Loqs-PD. This was shown by fluorescence microscopy of cells transfected with various GFP-Loqs-PD constructs and flies stably expressing those. As shown by FRAP experiments and treatment with hexanediol, the condensates exhibit a partially liquid-like nature probably composed of a mobile and immobile fraction and their formation is reversible. Furthermore, via immunostaining, it was possible to show that Loqs-PD and Dcr-2 localize to the same condensates. The proposed model (Figure 18) for the co-condensation of Loqs-PD, Dcr-2 and dsRNA illustrates that the role of Ago2 in the formation of these condensates is to be determined in the future. Ago2 could be part of the condensates formed by Loqs-PD and Dcr-2 as a scaffold protein or only transiently. Yet unsuccessful attempts to generate a full length Ago2 fusion protein that is not prone to proteolysis, made it difficult to examine the localization of Ago2 by live cell imaging. In cells stably expressing the N-terminus of Ago2, structures resembling condensates have been observed though more of a solid-like nature. Phase separation of the N-terminus of Ago2 has been shown *in vitro* as well as co-condensation with Loqs-PD and dsRNA (manuscript in preparation) thus it is highly likely that Ago2 is part of the condensate, too.

The greatest limitation for this study was the problem of generating the Ago2 fusion with a fluorescent protein as it obviously changed the biochemical behavior of the full-length protein. Major improvements or the development of completely new strategies for the visualization of the localization of Ago2 *in vivo* have to be implemented in the future course of the project. The role of dsRNA or in particular the amount of dsRNA needed for condensate formation can be examined further. However, it is difficult to estimate the amount of dsRNA present in cells. In this study, the addition of exogenous RNA to the cells did not change number or morphology of Loqs-PD condensates. Moreover, insights into the 3D structure especially of the intrinsically disordered domains of both Loqs-PD and Ago2 are very limited at the moment. Solving the 3D structure could support the understanding of the role of the IDR for condensate formation of these proteins, their molecular function and their homologs in other organisms.
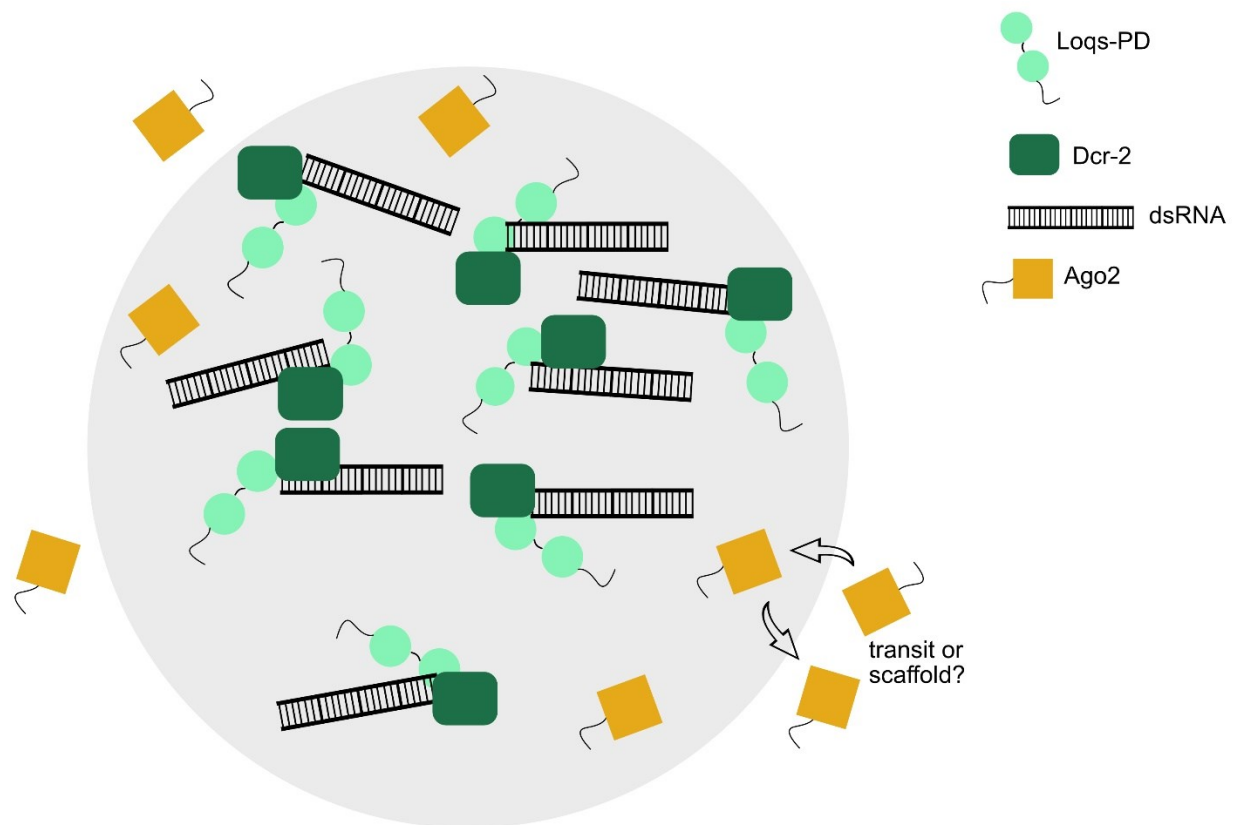
Figure 19. Proposed model of co-condensation of Loqs-PD, Dcr-2, dsRNA and Ago2. In the present work, it has been shown that Loqs-PD (intrinsically disordered N-terminus in black; light green spheres depict the two dsRBDs connected by the flexible linker in black) and Dcr-2 (dark green rectangle) colocalize to the same cytoplasmic condensate (grey sphere). In this drawing they are in complex together processing dsRNA (black). The role and localization of Ago2 (folded part of the protein depicted as an orange square, intrinsically disordered N-terminus in black) still has to be resolved. It could be part of the condensate formed by Loqs-PD and Dcr-2 as a scaffold protein or transiently. *This is a schematic drawing, not drawn to scale.*

4   Materials and Methods

Cell culture

The *Drosophila melanogaster* S2 cells were cultured in Schneider's medium (Bio&Sell) with 10 % FBS (Sigma) and Penicillin/Streptomycin (ThermoFisher Scientific) at 25 °C. The cells were split weekly by diluting them 1:10 into fresh medium.

The inducible Loqs in the *r2d2* ko cell line (Clone K54) and the inducible Dcr-2 clone 1 cell line were generated genome editing at the N-terminus of the protein of interest via a PCR-based CRISPR/Cas9 protocol developed in the Förstemann-lab (Böttcher et al., 2014; Kunzelmann et al., 2016).

For transient transfections, the specific plasmids were transfected with a concentration of 500 ng plasmid in 500 µl cell culture well (24-well plate) at a cell culture density of 1.5×10^6 cells/ml and the cells were examined at day 3 post transfection.

For the treatment with 1,6-hexandediol, the cells were transfected 3 days prior to the treatment. On treatment-day the cells were split 1:5 into fresh medium containing 10% 1,6-hexandediol and subsequently examined via microscopy.

Cloning strategies

GFP-Loqs-PD variants

The plasmid backbone (pKF254) used for the cloning of GFP-Loqs-PD variants was derived from pKF63 (Förstemann et al., 2007). A monomeric GFP variant (muGFP) and different Loqs-PD constructs were cloned into the vector by restriction digest. The Loqs-PD wild type sequence of the N-terminus was generated via PCR from a template plasmid whereas all of the other variants (Loqs-PD N-terminus with Q or N or Q/N→A, Loqs-PD with dsRBD1 and/or dsRBD2 KK→AA, Loqs-PD C-terminus) were dsDNA sequences ordered from IDT Integrated DNA Technologies and further used for cloning. Most of the Loqs-PD constructs also exist with a T7-tag instead of GFP (see plasmid list).

Fusion protein Ago2 with tdTomato, mCherry, GFP

The tdTomato-Ago2 plasmid (pRB92) was cloned via different cloning steps including the generation of tdTomato plasmid (pRB91) combined with the coding sequence of Ago2 from the pAFS-Ago2 (purchased from addgene). pRB91 also served as a backbone for cloning the tdTomato-Ago2-ΔN constructs and it was used to generate the mCherry plasmid (pTG2) by

exchanging the tdTomato sequence with mCherry. pTG2 was the starting point for the mCherry-Ago2 fusions. pLT2 was used as a backbone to generate the GFP-Ago2 plasmid.

Immunostaining

For the immunostaining of the cells, cells were harvested at 5500 g for 10 min and washed once with 1X PBS. The cells were applied to a poly-L-lysine slide for 45 min to settle down and adhere to the surface, then fixed with 1X PBS + 3.6 % formaldehyde for 3 min. Subsequently, the cells were washed 10 min with 1X PBS + 1 % Triton and afterwards blocked 2x 40 min in 1X PBS + 1 % Triton + 1 % BSA (bovine serum albumin). The cells were incubated with the primary antibody diluted in 1X PBS + 1 % Triton + 1 % BSA overnight in the cold room. The next day, cells were washed 3x for one hour with 1X PBS + 1 % Triton + 1 % BSA and incubated with the secondary antibody (coupled to a fluorophore) overnight in the cold room. To avoid fading of the fluorophore, the incubations with the fluorophore were carried out in the dark (covered with aluminum foil). On day three, the cells were washed again 3x for one hour with 1X PBS + 1 % Triton + 1 % BSA and then covered with mounting medium containing DABCO (1,4-diazabicyclo [2.2.2] octane) to prevent fading of the fluorescent signal and DAPI (4',6-diamidino-2-phenylindole) to stain the DNA. The slides were examined immediately or stored in the fridge. I did not notice fading of the fluorescence signal due to storage in the fridge.

Confocal microscopy and fluorescence recovery after photobleaching (FRAP)-assay

Imaging of GFP-Loqs-PD condensates in S2-cells and FRAP-assays were performed using a Zeiss LSM710 confocal laser scanning microscope with a 63X oil immersion objective. For live cell microscopy, the cells were placed in a chambered polymer coverslip at least two hours before the microscopy session or the day before for FRAP-assays in order that the cells tightly adhere to the bottom of the slide. For bleaching the GFP-Loqs-PD condensates during the FRAP assay, a circular region of interest (ROI) was defined around the condensate and bleached at a wavelength of 488 nm and 561 nm with full laser power. Bleaching started after the recording of 3 scans, the ROI was bleached and the recovery of the fluorescence was recorded.

The images were processed with Fiji (ImageJ) and the analysis of the FRAP-assays was conducted using the Stowers-ImageJ-Plugins.

Small RNA libraries

To generate small RNA libraries, total RNA was extracted from cell culture cells with the TRIzole reagent according to the manufacturer's protocol (Life Technologies). Oxidation of the RNA (without the step of the β-elimination) as well as the small RNA library preparation was performed according to the protocol developed in the Förstemann lab available on the intern data server (endo_siRNA_analysis_RB 01032023.docx) with the ZR small-RNA PAGE Recovery Kit (Zymo Research).

RNA isolation and cDNA synthesis for qPCR

RNA was isolated with TRIzole reagent according to the manufacturer's protocol (Life Technologies). Afterwards, the RNA was treated with DNase and purified with the RNA Clean and Concentrator Kit (Zymo Research). cDNA was synthesized using oligo DT and SuperScript Transcriptase (ThermoFisher Scientific). The qPCR was carried out in a technical triplicate.

qPCR reaction mix:

5 µl	SYBR Green PCR Master mix (ThermoFisher Scientific)
0.5 µl	sense primer (5 µM)
0.5 µl	antisense primer (5 µM)
0.1 µl	bromphenolblue
1.9 µl	H_2O
2.0 µl	cDNA template

qPCR program:

Step 1:	50 °C	10 s
Step 2:	95 °C	3 min
Step 3:	95 °C	30 s
Step 4:	59 °C	30 s
Step 5:	72 °C	42 s back to Step 3, 40x

Melting curve from 59 – 98 °C in 1 °C steps, 6 s each

The data was collected by TOptical thermo cycler (analytikjena) and the Ct-values were calculated by the qPCRsoft 3.4 software (analytikjena). Data analysis and calculations were performed in Microsoft Excel.

Protein isolation from cell culture cells for western blots

The cells (500 µl) were harvested at 5500 g for 10 minutes and washed with 1X PBS twice. The cell pellet was resuspended in 50 µl (1X PBS + 8 M Urea) and boiled at 95 °C for 10 min. Afterwards, the boiled cells were centrifuged for 10 min at maximum speed to separate the soluble from the insoluble fraction. The supernatant was transferred to a new reaction tube. The protein concentrations were measured with Bradford-assay and the desired amount was loaded on the polyacrylamide gel for a western blot.

Alternatively, cells were harvested and washed twice (as described above), boiled in 1X SDS loading buffer and directly loaded on the polyacrylamide gel.

Recombinant protein expression and purification Ago2 (1-413 aa)

The MBP-Ago2 (1-413 aa) plasmid (pSM2) was transformed into JM109 competent cells. The next day, a 15 ml day culture (37 °C) was inoculated and from this a 200 ml overnight culture was inoculated (37 °C). The next day, the 200 ml culture was diluted to 1000 ml (OD_{600}=0.42) and put to 23 °C until an OD_{600} of 0.65 was reached. At OD_{600}=0.65, the protein expression was induced with 1 M IPTG and put on 23 °C overnight. The cells were harvested at 4500 g for 13 min at 4 °C. The cell pellet was snap frozen and stored at -80 °C. For the lysis and first purification step with a gravity flow column with Ni-NTA agarose beads, the pellets were thawed in ice water and resuspended in lysis buffer (1X PBS, 1 % Triton, 1 mM DTT, Protease Inhibitor without EDTA, H_2O; pH 7-7.5). 1mg/ml lysozyme was added and incubated rolling for 30 min at 4 °C. The lysate was sonicated 4x 30 s with breaks, 20 % amplitude. The lysate was centrifuged for 20 min at 4460 g, the supernatant was transferred to a fresh reaction tube and centrifuged again. The supernatant was filtered (Chromafil GF100/25, Macherey-Nagel). The Protino Ni-NTA agarose (Invitrogen) beads were equilibrated with washing buffer (lysis buffer without protease inhibitor; pH 7-7.5). The equilibrated beads were incubated with the filtered lysate rolling for 60 min at 4 °C and then centrifuged for 2 min at 2000 g. The beads were taken up in washing buffer and loaded onto the column. The column was washed with washing buffer and the protein was eluted with imidazole-containing elution buffer (1X PBS, 0.1 % Triton, 1 mM DTT, 250 mM imidazole, H_2O; pH 7-7.5). Afterwards. the beads were washed again with washing buffer. The protein concentration of the different samples taken during the process were measured with Bradford-assay and loaded onto a polyacrylamide gel.

For subsequent purification of the elution fraction from the purification with the Ni-NTA agarose beads with the streptactin superflow beads (IBA Lifescience), the beads were equilibrated with

the washing buffer. The equilibrated beads were incubated with the elution fraction rolling for 60 min at 4 °C. The beads were centrifuged for 2 min at 2000. The beads were taken up in washing buffer and loaded onto the column. The column was washed with washing buffer and the protein was eluted with biotin-containing elution buffer (1X PBS, 0.1 % Triton, 1 mM DTT, 2.5 mM biotin, H_2O; pH 7-7.5). The column was washed again with washing buffer and the protein concentration of the different samples taken during the process were measured with Bradford-assay and loaded onto a polyacrylamide gel.

Plasmids used for experiments performed in this study

Name	Description	Lab internal number
pSM2	MBP-Ago2 N-term (1-413aa)	575
pSM11	GFP-Loqs-PD wild type	631
pSM14	GFP-Loqs-PD Q/N→A	634
pSM16	GFP-Loqs-PD both dsRBDs KK→AA	636
pSM19	GFP-Loqs-PD Q/N→A, both dsRBDs KK→AA	637
pSM41	GFP-Loqs-PD dsRBD2 KK→AA	665
pSM42	GFP-Loqs-PD dsRBD1 KK→AA	666
pSM49	mCherry-Ago2	690
pSM56	Ago2(1-413aa)-mCherry-Ago2(413-1208aa)	704
pSM58	Ago2(1-386aa)-mCherry-Ago2 (387-1208aa)	705
pTG1	GFP-Ago2	689
pTG2	mCherry	688
pLT2	muGFP	620
pRB91	tdTomato	606
pRB92	tdTomato-Ago2	609

Plasmids used for intermediate cloning steps and other

Name	Description	Lab internal number
pSM1	MBP-Loqs (105 nt)	566
pSM3	Loqs-PD wild type	621
pSM4	Loqs-PD N-term with Q→A	622
pSM5	Loqs-PD N-term with N→A	623
pSM6	Loqs-PD N-term with Q/N→A	624
pSM7	GS-linker (no N-term), + Loqs-PD, dsRBD1+2, C-term	625
pSM8	Loqs-PD both dsRBDs KK→AA	626
pSM9	Loqs-PD Q/N→A, both dsRBDs KK→AA	627
pSM10	GS-linker (no N-term), Loqs-PD both dsRBDs KK→AA, C-term	630
pSM12	GFP-Loqs-PD Q→A	632
pSM13	GFP-Loqs-PD N→A	633
pSM15	GFP-GS-linker-Loqs-PD dsRBDs, C-term	635
pSM17	GFP-Loqs-PD Q→A, both dsRBDs KK→AA	637
pSM18	GFP-Loqs-PD N→A, both dsRBDs KK→AA	638
pSM20	GFP-GS-linker (no N-term), Loqs-PD both dsRBDs KK→AA, C-term	640
pSM21	T7-tag-Loqs-PD wildtype	646
pSM22	T7-tag-Loqs-PD Q→A	647
pSM23	T7-tag-Loqs-PD N→A	648
pSM24	T7-tag-Loqs-PD Q/N→A	649
pSM25	T7-tag-GS-linker (no N-term), + Loqs-PD, dsRBD1+2, C-term	650
pSM26	T7-tag-Loqs-PD both dsRBDs KK→AA	651
pSM27	T7-tag-Loqs-PD Q→A, both dsRBDs KK→AA	652
pSM28	T7-tag-Loqs-PD N→A, both dsRBDs KK→AA	653

pSM29	T7-tag- Loqs-PD Q/N→A, both dsRBDs KK→AA	654
pSM30	T7-tag- GS-linker (no N-term), + Loqs-PD, both dsRBDs KK→AA, C-term	655
pSM31	Loqs-PD N→A, both dsRBDs KK→AA	628
pSM32	Loqs-PD Q/N→A, both dsRBDs KK→AA	629
pSM35	GFP-Loqs-PD, no C-term	656
pSM36	GFP- Loqs-PD Q/N→A, no C-term	657
pSM37	GFP-Loqs-PD both dsRBDs KK→AA, no C-term	658
pSM38	GFP-Loqs-PD Q/N→A, both dsRBDs KK→AA, no C-term	659
pSM39	Loqs-PD dsRBD1 KK→AA	663
pSM40	Loqs-PD dsRBD2 KK→AA	664
pSM43	tdTomato-Ago2(414-1208aa)	676
pSM44	tdTomato-Ago2(387-1208aa)	677
pSM45	GFP-Loqs-PD N-term + dsRBD1	678
pSM46	GFP-Loqs-PD N-term + dsRBD2 KK→AA	679
pSM47	GFP-Loqs-PD N-term + dsRBD2	680
pSM48	GFP-Loqs-PD N-term + dsRBD1 KK→AA	681
pSM50	mCherry-Ago2(414-1208aa)	696
pSM51	mCherry-Ago2(387-1208aa)	697
pSM52	mCherry-Ago1	698
pSM53	GFP-Ago1	699
pSM54	mCherry-Ago2(414-1208aa; gBlock)	700
pSM55	Ago2(72-413aa)-mCherry- Ago2(414-1208aa; gBlock)	702
pSM57	mCherry-Ago2(387-1208aa)	706
pLT1	T7-tag	619

Fly lines (generated by Klaus Förstemann and Mihai-Alin Baur)

Lab internal number	Phenotype
98	w; +; attP2: pRB10
212	yw; +; attP86Fb(3xP3-DsRed): pSM11
217	yw; +; attP86Fb(3xP3-DsRed): pSM41
218	yw; +; attP86Fb(3xP3-DsRed): pSM42

Primer list

Lab internal number	Name	Sequence
1631	WT-Check-Fwd Dcr2	CTCTGTCACCGGCTTCTTTG
1632	WT-Check-Rev Dcr2	GCTCTTCGTTAGGTGGTCAA
1657	Col_PCR_#551_Fwd	TATTTCCAGGGAGCAGCCTC
1658	Col_PCR_#551_Rev	CCAAGGGGTTATGCTAGTTA
1705	551 MBP --> lig sense	ATTAA GCCGCCAGT CCG AA
1739	Ago2_antisense	ACGCTGTTGGTAGCCACCTT
1740	Ago2_as_no2	ATT GTT CCG CGC TTA ATG CT
1741	Ago2_as_no3	ATGGCCACCTTGTTGACCTTGTTTAG
1758	CMV_Tomato_myc_seq_as	caacaacaattgcattcattttatgtttcag
1759	Tomato_Stop_delete_as	GGCCGCgaggtaccGCCCAAGTCTTCTTCAGAAATAAGTTTTTGTTCCATagatctccT
1760	Tomato_Stop_delete_sense	GTACAggagatctATGGAACAAAAACTTATTTCTGAAGAAGACTTGGGCggtacctcGC
1761	Tomato_myc_sense	GAGCTGTACAggagatctATGGAAC
1772	Kpn_Gs-linker_Aat_as_new	cTCCTGCACTAGAACCGCTACTACCggtac
1773	T7_tag_sense_new	GATCCACCATGGCCAGCATGACCGGCGGCCAGCAGATGGGCGGTACCGC
1774	T7_tag_antisense_new	ggccgcGGTACCGCCCATCTGCTGGCCGCCGGTCATGCTGGCCATGGTG
1791	ColPCR_Seq_pKF254_s	GGTTTCTCAACAAAGTTGGCGTCG
1792	ColPCR_Seq_pUC18_sense	GCCTCTTCGCTATTACGCCA
1793	ColPCR_Seq_pUC18_as_1	TACACTTTATGCTTCCGGCT
1796	Primer_pKF254_new	GCAACGGAACAAAGGTTTCTCA

1797	Dcr-2_cDNA_sense	GATATGACTGCGACAGTCAA
1798	Dcr-2_cDNA_as	TTCTAGTGGTCTGGGCATGT
1801	Seq_Loqs Cloning_as	TTAGCAGCTCTTGCAGAATG
1804	pUC18_seq_sense	CGGCATCAGAGCAGATTGTA
1805	Loqs_Cterm_sense	AGGAGACGGCAATGCCAATG
1806	Loqs_Cterm_as	CATTGGCATTGCCGTCTCCT
1843	muGFP_sense	ACCACTACCTGTCAACTCAA
1860	qPCR_Loqs_sense_1	CGCCTGCTCGATACTCAACT
1861	qPCR_loqs_as_1a	CTGTCGCTGATTTTGCCCG
1862	qPCR_loqs_as_1b	GTCGCTGATTTTGCCCGAAT
1863	qPCR_loqs_sense_2	TGGAGGGCGAAGTGAGTATC
1864	qPCR_loqs_as_2	TGCTTGTGGGTTAGATCTTGATG
1865	KpnI+Loqs_sense	AGAAGGTACCATGGACCAGGAGAA
1866	Loqs_deltaC_cloning_as	AAGCGGCCGCTTCAATCGATGGGAGTCTCCTGCA
1903	Loqs_Tagging_WT-check_s	GTCTGGCAACCACAAATATC
1904	Loqs_Tagging_WT-check_as	AGGCCGACTCCACCTTGTAA
1905	T7_Loqs_5'UTR_sense	taatacgactcactatagggTCGTGTGTGCGTCTGGATTT
1906	T7_Loqs_5'UTR_as	taatacgactcactatagggAGCACCCTTCACCGGACTA
1907	Kpn+Loqs QN/A_sense	AGAAGGTACCATGGACGCGGAGGC
1935	CRISPR_loqs_Blunt 10	CCTATTTTCAATTTAACGTCGTATCGATTTTTCAAAACCAGTTTAAGAGCTATGCTG
1937	Ago2dN_folded_sense	gatGCGGCCGCatgCCCCATTACCATTACCGCC
1938	Ago2dN(N=1-413aa)_sense	gatGCGGCCGCATCTGGACCTTGACCTGTCC
1939	Ago2dN_as	tcaTCTAGATCAGACAAAGTACATGGGGT
1940	Ago2_sequencing_sense	ATGGCATGAAGTTTCTGGAG
1941	Ago2_sequencing_as	CTCCAGAAACTTCATGCCAT
1975	Seq_tomato-Ago2dN_as	TTGTTCAAATGCCTGTCTG
1980	Primer_sense_Ago 1+KpnI	gatGGTACCATGTATCCAGTTGGACAACA
1981	Primer_as_Ago1+NotI	tcaGCGGCCGCTTAGGCAAAGTACATGACCT
2013	mCherry+AgeI+Kozak_sense	gctACCGGTccaccATGGTGTCCAAGGGCGAAGA
2014	mCherry+NotI_as	aatGCGGCCGCCAGACTGGAGTTCGAGGTAC

2015	ColPCR_Sq_Primer _pRB91_s	GGTTTCTCAACAAAGTTGGCGTCG
2021	Ago2_CDS_s	AATACTTCCAGCACAACCTG
2022	mCherry_seq_as	CATCCATGCCTCCGGTGCTG
2023	mCherry_seq_s	TTATCAAGGAGTTCATGCGC
2025	NotI+2nt+dN(1-413a)Ago2_s	GATGCGGCCGCAAATCTGGACCTTGACCTGTCC
2026	NotI+2nt+dNAgo2(folded)_s	GATGCGGCCGCAACCCCATTACCATTACCGCC
2029	ColonyPCR_Ago2_sense	TTGCTGCGTGATTGTGGTGA
2030	Ago1CDS_seq_sense	CCGACTTCAACAACGATTCG
2031	Ago1CDS_seq_as	CGAATCGTTGTTGAAGTCGG
2032	BamHI-ATG-Nshort-Ago2_s	ACAGGATCCATGCGTGCATCTGGGTTTCAGCA
2033	BglII-ATG-Nterm-Ago2_s	acaAGATCTatgggaaaaaaagataagaa
2034	AgeI-Nterm-Ago2_as	GTCACCGGTAGTTGATGCCTACTTGCCCG
2035	mCherry_sense	TTGTAGAGCAATATGAGCGC
2036	Ago2_seq_sense	CCGCATTGCCAACGATTTTA
2037	Ago1_seq_sense	TGGAGAACGGACAGACCGTA
2043	Ago2_Nterm_int_check_as	TGTGGTTGTTGCAGCTGCTG
2044	Col_UbiProm_s	TGAAATTCGCAGTGACGCAT
2045	Col_PCR_Ago2_Nterm_as	TCTGTGCAGTCCATCCTTCTGC
2046	mCherry_sequencing_as	GAAGAGGATAATATGGCGAT
2047	mCherry_seq2_as	GGCAAATGGGAGAGGACCAC
2048	Ago2 Nterm as aa387	GTCACCGGTCAGCCTGCTGTTGCTGAGGT
2049	PCR neo-resistance as	GCAATATCACGGGTAGCCAA
2057	Ago2_sequencing_sense	AGTGAGACCTTCGAACACGA
336	optimized gRNA scaffold	GTTTaAGAGCTATgctgGAAAcagcaTAGCAAGTTtAAATAAGGCTAGTCCGTTATCAACTTGAAAAAGTGGCACCGAGTCGGTGC
811	CRISPR_N_Dcr2_new	cctattttcaatttaacgtcgGAGCGAAGATATGGAAGATGgtttaagagctatgctg
254	as_scaffold_pol3ter	gcttattctcAAAAAAGCACCGACTCGGTGCCACT
422	Dcr2_Nterm_target_s	ATCGTAAATTATTTGACTTCAAATTGTAATATCAAAATATCCCGAAGACTCTGTAACCAAGAGCGAAGATGaagttcctatactttctagagaataggaacttcCATATG

423	Dcr2_Nterm_target _as	gattttgttaattattttgcaataagcgagagcgcaagccaattcattttacCTTG ATTTCCACATCTTCACCGCCGCTTGGAGCAGC
1524	CRISPR_Loqs_Nt	cctattttcaatttaacgtcgGTGCAAAACAAGAACACCAgtttaagagct atgctg
1525	Loqs_Ntag_s	ccgaaattttaaacagATACACACCGAATCCTCCCGAAAACCGTGC AAAACAAGAACACCgaagttcctatactttctagagaataggaacttccata tg
1526	Loqs_Ntag_as	CTGGATGTGGAGGTTCTGTAGCTGCTGCGGCAAGCTGGAGCC GTGGAAATTCTCCTGGTCaccgccgcttggagcagcTGGAGA
1360	rp49 A2	ATCGGTTACGGATCGAACA
1361	rp49 B2	ACAATCTCCTTGCGCTTCTT

5 Literature

Ader, C., Frey, S., Maas, W., Schmidt, H. B., Gorlich, D., & Baldus, M. (2010). Amyloid-like interactions within nucleoporin FG hydrogels. *Proc Natl Acad Sci U S A*, *107*(14), 6281-6285. https://doi.org/10.1073/pnas.0910163107

Alberti, S., & Dormann, D. (2019). Liquid-Liquid Phase Separation in Disease. *Annu Rev Genet*, *53*, 171-194. https://doi.org/10.1146/annurev-genet-112618-043527

Alberti, S., Gladfelter, A., & Mittag, T. (2019). Considerations and Challenges in Studying Liquid-Liquid Phase Separation and Biomolecular Condensates. *Cell*, *176*(3), 419-434. https://doi.org/10.1016/j.cell.2018.12.035

Alberti, S., Halfmann, R., King, O., Kapila, A., & Lindquist, S. (2009). A systematic survey identifies prions and illuminates sequence features of prionogenic proteins. *Cell*, *137*(1), 146-158. https://doi.org/10.1016/j.cell.2009.02.044

Alberti, S., & Hyman, A. A. (2016). Are aberrant phase transitions a driver of cellular aging? *Bioessays*, *38*(10), 959-968. https://doi.org/10.1002/bies.201600042

Aravin, A. A., Hannon, G. J., & Brennecke, J. (2007). The Piwi-piRNA Pathway Provides an Adaptive Defense in the Transposon Arms Racev. *Science*, *318*, 761-764. https://doi.org/10.1126/science.1146484

Aravin, A. A., Lagos-Quintana, M., Yalcin, A., Zavolan, M., Marks, D., Snyder, B., Gaasterland, T., Meyer, J., & Tuschl, T. (2003). The small RNA profile during Drosophila melanogaster development. *Dev Cell*, *5*(2), 337-350. https://doi.org/10.1016/s1534-5807(03)00228-4

Aravin, A. A., Naumova, N. M., Tulin, A. V., Vagin, V. V., Rozovsky, Y. M., & Gvodzev, V. A. (2001). Double-stranded RNA-mediated silencing of genomic tandem repeats and transposable elements in the D. melanogaster germline. *Curr Biol*, *11*(13), 1017-1027. https://doi.org/10.1016/s0960-9822(01)00299-8

Banani, S. F., Lee, H. O., Hyman, A. A., & Rosen, M. K. (2017). Biomolecular condensates: organizers of cellular biochemistry. *Nat Rev Mol Cell Biol*, *18*(5), 285-298. https://doi.org/10.1038/nrm.2017.7

Banani, S. F., Rice, A. M., Peeples, W. B., Lin, Y., Jain, S., Parker, R., & Rosen, M. K. (2016). Compositional Control of Phase-Separated Cellular Bodies. *Cell*, *166*(3), 651-663. https://doi.org/10.1016/j.cell.2016.06.010

Baulcombe, D. (2004). RNA silencing in plants. *Nature*, *431*, 356-363.

Bentmann, E., Neumann, M., Tahirovic, S., Rodde, R., Dormann, D., & Haass, C. (2012). Requirements for stress granule recruitment of fused in sarcoma (FUS) and TAR DNA-binding protein of 43 kDa (TDP-43). *J Biol Chem*, *287*(27), 23079-23094. https://doi.org/10.1074/jbc.M111.328757

Bernstein, E., Caudy, A. A., Hammond, S. M., & Hannon, G. J. (2001). Role for a bidentate ribonuclease in the initation step of RNA interference. *Nature*, *409*, 363-366.

Berry, J., Brangwynne, C. P., & Haataja, M. (2018). Physical principles of intracellular organization via active and passive phase transitions. *Rep Prog Phys*, *81*(4), 046601. https://doi.org/10.1088/1361-6633/aaa61e

Böttcher, R., Hollmann, M., Merk, K., Nitschko, V., Obermaier, C., Philippou-Massier, J., Wieland, I., Gaul, U., & Förstemann, K. (2014). Efficient chromosomal gene modification with CRISPR/cas9 and PCR-based homologous recombination donors in cultured Drosophila cells. *Nucleic Acids Res*, *42*(11), e89. https://doi.org/10.1093/nar/gku289

Bracha, D., Walls, M. T., & Brangwynne, C. P. (2019). Probing and engineering liquid-phase organelles. *Nat Biotechnol*, *37*(12), 1435-1445. https://doi.org/10.1038/s41587-019-0341-6

Brangwynne, C. P., Eckmann, C. R., Courson, D. S., Rybarska, A., Hoege, C., Gharakhani, J., Jülicher, F., & Hyman, A. A. (2009). Germline P Granules Are Liquid Droplets That Localize by Controlled Dissolution/Condensation. *Science*, *324*, 1729-1732. https://doi.org/10.1126/science.1172046

Brangwynne, Clifford P., Tompa, P., & Pappu, Rohit V. (2015). Polymer physics of intracellular phase transitions. *Nature Physics*, *11*(11), 899-904. https://doi.org/10.1038/nphys3532

Brennecke, J., Aravin, A. A., Stark, A., Dus, M., Kellis, M., Sachidanandam, R., & Hannon, G. J. (2007). Discrete small RNA-generating loci as master regulators of transposon activity in Drosophila. *Cell*, *128*(6), 1089-1103. https://doi.org/10.1016/j.cell.2007.01.043

Burke, K. A., Janke, A. M., Rhine, C. L., & Fawzi, N. L. (2015). Residue-by-Residue View of In Vitro FUS Granules that Bind the C-Terminal Domain of RNA Polymerase II. *Mol Cell*, *60*(2), 231-241. https://doi.org/10.1016/j.molcel.2015.09.006

Cenik, E. S., & Zamore, P. D. (2011). Argonaute proteins. *Curr Biol*, *21*(12), R446-449. https://doi.org/10.1016/j.cub.2011.05.020

Cheloufi, S., Dos Santos, C. O., Chong, M. M., & Hannon, G. J. (2010). A dicer-independent miRNA biogenesis pathway that requires Ago catalysis. *Nature*, *465*(7298), 584-589. https://doi.org/10.1038/nature09092

Chen, Y. G., & Hur, S. (2022). Cellular origins of dsRNA, their recognition and consequences. *Nat Rev Mol Cell Biol*, *23*(4), 286-301. https://doi.org/10.1038/s41580-021-00430-1

Chendrimada, T. P., Gregory, R. I., Kumaraswamy, E., Norman, J., Cooch, N., Nishikura, K., & Shiekhattar, R. (2005). TRBP recruits the Dicer complex to Ago2 for microRNA processing and gene silencing. *Nature*, *436*(7051), 740-744. https://doi.org/10.1038/nature03868

Chong, P. A., Vernon, R. M., & Forman-Kay, J. D. (2018). RGG/RG Motif Regions in RNA Binding and Phase Separation. *J Mol Biol*, *430*(23), 4650-4665. https://doi.org/https://doi.org/10.1016/j.jmb.2018.06.014

Colaianni, D., & De Pitta, C. (2022). The Role of microRNAs in the Drosophila Melanogaster Visual System. *Front Cell Dev Biol*, *10*, 889677. https://doi.org/10.3389/fcell.2022.889677

Czech, B., Malone, C. D., Zhou, R., Stark, A., Schlingeheyde, C., Dus, M., Perrimon, N., Kellis, M., Wohlschlegel, J. A., Sachidanandam, R., Hannon, G. J., & Brennecke, J. (2008). An endogenous small interfering RNA pathway in Drosophila. *Nature*, *453*(7196), 798-802. https://doi.org/10.1038/nature07007

Dai, Q., Smibert, P., & Lai, E. C. (2012). Exploiting Drosophila genetics to understand microRNA function and regulation. *Curr Top Dev Biol*, *99*, 201-235. https://doi.org/10.1016/B978-0-12-387038-4.00008-2

Denli, A. M., Tops, B. B. J., Plasterk, R. H. A., Ketting, R. F., & Hannon, G. J. (2004). Processing of primary microRNAs by the Microprocessor complex. *Nature*, *432*, 231-235.

Duster, R., Kaltheuner, I. H., Schmitz, M., & Geyer, M. (2021). 1,6-Hexanediol, commonly used to dissolve liquid-liquid phase separated condensates, directly impairs kinase and phosphatase activities. *J Biol Chem*, *296*, 100260. https://doi.org/10.1016/j.jbc.2021.100260

Eamens, A., Wang, M. B., Smith, N. A., & Waterhouse, P. M. (2008). RNA silencing in plants: yesterday, today, and tomorrow. *Plant Physiol*, *147*(2), 456-468. https://doi.org/10.1104/pp.108.117275

Elkayam, E., Kuhn, C. D., Tocilj, A., Haase, A. D., Greene, E. M., Hannon, G. J., & Joshua-Tor, L. (2012). The structure of human argonaute-2 in complex with miR-20a. *Cell*, *150*(1), 100-110. https://doi.org/10.1016/j.cell.2012.05.017

Eulalio, A., Behm-Ansmant, I., Schweizer, D., & Izaurralde, E. (2007). P-body formation is a consequence, not the cause, of RNA-mediated gene silencing. *Mol Cell Biol*, *27*(11), 3970-3981. https://doi.org/10.1128/MCB.00128-07

Evers, M., Huttner, M., Dueck, A., Meister, G., & Engelmann, J. C. (2015). miRA: adaptable novel miRNA identification in plants using small RNA sequencing data. *BMC Bioinformatics*, *16*, 370. https://doi.org/10.1186/s12859-015-0798-3

Fire, A., Xu, S., Montgomery, M. K., Kostas, S. A., Driver, S. E., & Mello, C. C. (1998). Potent and specific genetic interference by double-stranded RNA in Caenorhabditis elegans. *Nature*, *391*, 806-811.

Flory, P. J. (1953). *Principles of Polymer Chemisty*. Cornell University Press.

Förstemann, K., Horwich, M. D., Wee, L., Tomari, Y., & Zamore, P. D. (2007). Drosophila microRNAs are sorted into functionally distinct argonaute complexes after production by dicer-1. *Cell*, *130*(2), 287-297. https://doi.org/10.1016/j.cell.2007.05.056

Förstemann, K., Tomari, Y., Du, T., Vagin, V. V., Denli, A. M., Bratu, D. P., Klattenhoff, C., Theurkauf, W. E., & Zamore, P. D. (2005). Normal microRNA maturation and germ-line stem cell maintenance requires Loquacious, a double-stranded RNA-binding domain protein. *PLoS Biol*, *3*(7), e236. https://doi.org/10.1371/journal.pbio.0030236

Franzmann, T. M., & Alberti, S. (2019a). Prion-like low-complexity sequences: Key regulators of protein solubility and phase behavior. *J Biol Chem*, *294*(18), 7128-7136. https://doi.org/10.1074/jbc.TM118.001190

Franzmann, T. M., & Alberti, S. (2019b). Protein Phase Separation as a Stress Survival Strategy. *Cold Spring Harb Perspect Biol*, *11*(6). https://doi.org/10.1101/cshperspect.a034058

Ghildiyal, M., & Zamore, P. D. (2009). Small silencing RNAs: an expanding universe. *Nat Rev Genet*, *10*(2), 94-108. https://doi.org/10.1038/nrg2504

Golden, D. E., Gerbasi, V. R., & Sontheimer, E. J. (2008). An inside job for siRNAs. *Mol Cell*, *31*(3), 309-312. https://doi.org/10.1016/j.molcel.2008.07.008

Guo, L., & Shorter, J. (2015). It's Raining Liquids: RNA Tunes Viscoelasticity and Dynamics of Membraneless Organelles. *Mol Cell*, *60*(2), 189-192. https://doi.org/10.1016/j.molcel.2015.10.006

Guo, Q., Liu, Q., Smith, N. A., Liang, G., & Wang, M.-B. (2016). RNA Silencing in Plants: Mechanisms, Technologies and Applications in

Horticultural Crops. *Current Genomics*, *17*, 476-489. https://doi.org/10.2174/1389202917666160520010

Haase, A. D., Jaskiewicz, L., Zhang, H., Laine, S., Sack, R., Gatignol, A., & Filipowicz, W. (2005). TRBP, a regulator of cellular PKR and HIV-1 virus expression, interacts with Dicer and functions in RNA silencing. *EMBO Rep*, *6*(10), 961-967. https://doi.org/10.1038/sj.embor.7400509

Hain, D., Bettencourt, B. R., Okamura, K., Csorba, T., Meyer, W., Jin, Z., Biggerstaff, J., Siomi, H., Hutvagner, G., Lai, E. C., Welte, M., & Muller, H. A. (2010). Natural variation of the amino-terminal glutamine-rich domain in Drosophila argonaute2 is not associated with developmental defects. *PLoS One*, *5*(12), e15264. https://doi.org/10.1371/journal.pone.0015264

Hartig, J. V., Esslinger, S., Bottcher, R., Saito, K., & Forstemann, K. (2009). Endo-siRNAs depend on a new isoform of loquacious and target artificially introduced, high-copy sequences. *EMBO J*, *28*(19), 2932-2944. https://doi.org/10.1038/emboj.2009.220

Huang, X., Fejes Toth, K., & Aravin, A. A. (2017). piRNA Biogenesis in Drosophila melanogaster. *Trends Genet*, *33*(11), 882-894. https://doi.org/10.1016/j.tig.2017.09.002

Hyman, A. A., Weber, C. A., & Julicher, F. (2014). Liquid-liquid phase separation in biology. *Annu Rev Cell Dev Biol*, *30*, 39-58. https://doi.org/10.1146/annurev-cellbio-100913-013325

Ipsaro, J. J., & Joshua-Tor, L. (2015). From Guide to Target: Molecular Insights into Eukaryotic RNAi Machinery. *Nat Struct Mol Biol*, *22*(1), 20-28.

Jain, A., & Vale, R. D. (2017). RNA phase transitions in repeat expansion disorders. *Nature*, *546*(7657), 243-247. https://doi.org/10.1038/nature22386

Jakob, L., Treiber, T., Treiber, N., Gust, A., Kramm, K., Hansen, K., Stotz, M., Wankerl, L., Herzog, F., Hannus, S., Grohmann, D., & Meister, G. (2016). Structural and functional insights into the fly microRNA biogenesis factor Loquacious. *RNA*, *22*(3), 383-396. https://doi.org/10.1261/rna.055426.115

Jaubert, S., Mereau, A., Antoniewski, C., & Tagu, D. (2007). MicroRNAs in Drosophila: the magic wand to enter the Chamber of Secrets? *Biochimie*, *89*(10), 1211-1220. https://doi.org/10.1016/j.biochi.2007.05.012

Ji, L., & Chen, X. (2012). Regulation of small RNA stability: methylation and beyond. *Cell Res*, *22*(4), 624-636. https://doi.org/10.1038/cr.2012.36

Jiang, F., Ye, X., Liu, X., Fincher, L., McKearin, D., & Liu, Q. (2005). Dicer-1 and R3D1-L catalyze microRNA maturation in Drosophila. *Genes Dev*, *19*(14), 1674-1679. https://doi.org/10.1101/gad.1334005

Jouravleva, K., Golovenko, D., Demo, G., Dutcher, R. C., Hall, T. M. T., Zamore, P. D., & Korostelev, A. A. (2022). Structural basis of microRNA biogenesis by Dicer-1 and its partner protein Loqs-PB. *Mol Cell*, *82*(21), 4049-4063 e4046. https://doi.org/10.1016/j.molcel.2022.09.002

Kadener, S., Rodriguez, J., Abruzzi, K. C., Khodor, Y. L., Sugino, K., Marr, M. T., 2nd, Nelson, S., & Rosbash, M. (2009). Genome-wide identification of targets of the drosha-pasha/DGCR8 complex. *RNA*, *15*(4), 537-545. https://doi.org/10.1261/rna.1319309

Kato, M., Han, T. W., Xie, S., Shi, K., Du, X., Wu, L. C., Mirzaei, H., Goldsmith, E. J., Longgood, J., Pei, J., Grishin, N. V., Frantz, D. E., Schneider, J. W., Chen, S., Li, L., Sawaya, M. R., Eisenberg, D., Tycko, R., & McKnight, S. L. (2012). Cell-free formation of RNA granules: low complexity sequence domains form dynamic fibers within hydrogels. *Cell*, *149*(4), 753-767. https://doi.org/10.1016/j.cell.2012.04.017

Kirilly, D., & Xie, T. (2007). The Drosophila ovary: an active stem cell community. *Cell Res*, *17*(1), 15-25. https://doi.org/10.1038/sj.cr.7310123

Koh, H. R., Kidwell, M. A., Ragunathan, K., Doudna, J. A., & Myong, S. (2013). ATP-independent diffusion of double-stranded RNA binding proteins. *Proc Natl Acad Sci U S A*, *110*(1), 151-156. https://doi.org/10.1073/pnas.1212917110

Kroschwald, S., Maharana, S., & Simon, A. (2017). Hexanediol: a chemical probe to investigate the material properties of membrane-less compartments. *Matters*. https://doi.org/10.19185/matters.201702000010

Kunzelmann, S., Böttcher, R., Schmidts, I., & Förstemann, K. (2016). A Comprehensive Toolbox for Genome Editing in Cultured Drosophila melanogaster Cells. *G3 (Bethesda)*, *6*(6), 1777-1785. https://doi.org/10.1534/g3.116.028241

Lancaster, A. K., Nutter-Upham, A., Lindquist, S., & King, O. D. (2014). PLAAC: a web and command-line application to identify proteins with prion-like amino acid composition. *Bioinformatics*, *30*(17), 2501-2502. https://doi.org/10.1093/bioinformatics/btu310

Lee, Y., Hur, I., Park, S. Y., Kim, Y. K., Suh, M. R., & Kim, V. N. (2006). The role of PACT in the RNA silencing pathway. *EMBO J*, *25*(3), 522-532. https://doi.org/10.1038/sj.emboj.7600942

Lee, Y., Jeon, K., Lee, J. T., Kim, S., & Kim, V. N. (2002). MicroRNA maturation: stepwise processing and subcellular localization. *EMBO J*, *21*(17), 4663-4670. https://doi.org/10.1093/emboj/cdf476

Lee, Y. S., Nakahara, K., Pham, J. W., Kim, K., He, Z., Sontheimer, E. J., & Carthew, R. W. (2004). Distinct Roles for Drosophila Dicer-1 and Dicer-2 in the siRNA/miRNA Silencing Pathways. *Cell*, *117*, 69-81.

Li, P., Banjade, S., Cheng, H. C., Kim, S., Chen, B., Guo, L., Llaguno, M., Hollingsworth, J. V., King, D. S., Banani, S. F., Russo, P. S., Jiang, Q. X., Nixon, B. T., & Rosen, M. K. (2012). Phase

transitions in the assembly of multivalent signalling proteins. *Nature*, *483*(7389), 336-340. https://doi.org/10.1038/nature10879

Li, Y. R., King, O. D., Shorter, J., & Gitler, A. D. (2013). Stress granules as crucibles of ALS pathogenesis. *J Cell Biol*, *201*(3), 361-372. https://doi.org/10.1083/jcb.201302044

Lim, A. K., & Kai, T. (2007). Unique germ-line organelle, nuage, functions to repress selfish genetic elements in Drosophila melanogaster. *Proc Natl Acad Sci U S A*, *104*, 6714-6719. https://doi.org/10.1073/pnas.0701920104

Lim, A. K., Tao, L., & Kai, T. (2009). piRNAs mediate posttranscriptional retroelement silencing and localization to pi-bodies in the Drosophila germline. *J Cell Biol*, *186*(3), 333-342. https://doi.org/10.1083/jcb.200904063

Lin, Y., Protter, D. S. W., Rosen, M. K., & Parker, R. (2015). Formation and Maturation of Phase Separated Liquid Droplets by RNA Binding Proteins. *Mol Cell*, *60*(2), 208-219.

Liu-Yesucevitz, L., Bilgutay, A., Zhang, Y. J., Vanderweyde, T., Citro, A., Mehta, T., Zaarur, N., McKee, A., Bowser, R., Sherman, M., Petrucelli, L., & Wolozin, B. (2010). Tar DNA binding protein-43 (TDP-43) associates with stress granules: analysis of cultured cells and pathological brain tissue. *PLoS One*, *5*(10), e13250. https://doi.org/10.1371/journal.pone.0013250

Liu, J., Valencia-Sanchez, M. A., Hannon, G. J., & Parker, R. (2005). MicroRNA-dependent localization of targeted mRNAs to mammalian P-bodies. *Nat Cell Biol*, *7*(7), 719-723. https://doi.org/10.1038/ncb1274

Liu, X., Jiang, F., Kalidas, S., Smith, D., & Liu, Q. (2006). Dicer-2 and R2D2 coordinately bind siRNA to promote assembly of the siRISC complexes. *RNA*, *12*(8), 1514-1520. https://doi.org/10.1261/rna.101606

Lund, E., Güttinger, S., Calado, A., Dahlberg, J. E., & Kutay, U. (2004). Nuclear Export of MicroRNA Precursors. *Science*, *303*, 95-98.

Malone, C. D., Brennecke, J., Dus, M., Stark, A., McCombie, W. R., Sachidanandam, R., & Hannon, G. J. (2009). Specialized piRNA pathways act in germline and somatic tissues of the Drosophila ovary. *Cell*, *137*(3), 522-535. https://doi.org/10.1016/j.cell.2009.03.040

Marques, J. T., Kim, K., Wu, P. H., Alleyne, T. M., Jafari, N., & Carthew, R. W. (2010). Loqs and R2D2 act sequentially in the siRNA pathway in Drosophila. *Nat Struct Mol Biol*, *17*(1), 24-30. https://doi.org/10.1038/nsmb.1735

Mirkovic-Hosle, M., & Forstemann, K. (2014). Transposon defense by endo-siRNAs, piRNAs and somatic pilRNAs in Drosophila: contributions of Loqs-PD and R2D2. *PLoS One*, *9*(1), e84994. https://doi.org/10.1371/journal.pone.0084994

Miyoshi, K., Miyoshi, T., Hartig, J. V., Siomi, H., & Siomi, M. C. (2010). Molecular mechanisms that funnel RNA precursors into endogenous small-interfering RNA and microRNA biogenesis pathways in Drosophila. *RNA*, *16*(3), 506-515. https://doi.org/10.1261/rna.1952110

Miyoshi, K., Okada, T. N., Siomi, H., & Siomi, M. C. (2009). Characterization of the miRNA-RISC loading complex and miRNA-RISC formed in the Drosophila miRNA pathway. *RNA*, *15*(7), 1282-1291. https://doi.org/10.1261/rna.1541209

Moazed, D. (2009). Small RNAs in transcriptional gene silencing and genome defence. *Nature*, *457*(7228), 413-420. https://doi.org/10.1038/nature07756

Murakami, T., Qamar, S., Lin, J. Q., Schierle, G. S., Rees, E., Miyashita, A., Costa, A. R., Dodd, R. B., Chan, F. T., Michel, C. H., Kronenberg-Versteeg, D., Li, Y., Yang, S. P., Wakutani, Y., Meadows, W., Ferry, R. R., Dong, L., Tartaglia, G. G., Favrin, G., . . . St George-Hyslop, P. (2015). ALS/FTD Mutation-Induced Phase Transition of FUS Liquid Droplets and Reversible Hydrogels into Irreversible Hydrogels Impairs RNP Granule Function. *Neuron*, *88*(4), 678-690. https://doi.org/10.1016/j.neuron.2015.10.030

Nakamura, M., Ando, R., Nakazawa, T., Yudazono, T., Tsutsumi, N., Hatanaka, N., Ohgake, T., Hanaoka, F., & Eki, T. (2007). Dicer-related drh-3 gene functions in germ-line development by maintenance of chromosomal integrity in Caenorhabditis elegans. *Genes Cells*, *12*(9), 997-1010. https://doi.org/10.1111/j.1365-2443.2007.01111.x

Nakanishi, K. (2022). Anatomy of four human Argonaute proteins. *Nucleic Acids Res*, *50*(12), 6618-6638. https://doi.org/10.1093/nar/gkac519

Nishida, K. M., Miyoshi, K., Ogino, A., Miyoshi, T., Siomi, H., & Siomi, M. C. (2013). Roles of R2D2, a cytoplasmic D2 body component, in the endogenous siRNA pathway in Drosophila. *Mol Cell*, *49*(4), 680-691. https://doi.org/10.1016/j.molcel.2012.12.024

Nitschko, V., Kunzelmann, S., Frohlich, T., Arnold, G. J., & Forstemann, K. (2020). Trafficking of siRNA precursors by the dsRBD protein Blanks in Drosophila. *Nucleic Acids Res*, *48*(7), 3906-3921. https://doi.org/10.1093/nar/gkaa072

Nott, T. J., Petsalaki, E., Farber, P., Jervis, D., Fussner, E., Plochowietz, A., Craggs, T. D., Bazett-Jones, D. P., Pawson, T., Forman-Kay, J. D., & Baldwin, A. J. (2015). Phase transition of a disordered nuage protein generates environmentally responsive membraneless organelles. *Mol Cell*, *57*(5), 936-947. https://doi.org/10.1016/j.molcel.2015.01.013

Okamura, K., Balla, S., Martin, R., Liu, N., & Lai, E. C. (2008). Two distinct mechanisms generate endogenous siRNAs from bidirectional transcription in Drosophila melanogaster. *Nat Struct Mol Biol*, *15*(6), 581-590. https://doi.org/10.1038/nsmb.1438

Okamura, K., Ishizuka, A., Siomi, H., & Siomi, M. C. (2004). Distinct roles for Argonaute proteins in small RNA-directed RNA cleavage pathways. *Genes Dev*, *18*(14), 1655-1666. https://doi.org/10.1101/gad.1210204

Palmer, W. H., & Obbard, D. J. (2016). Variation and Evolution in the Glutamine-Rich Repeat Region of Drosophila Argonaute-2. *G3 (Bethesda)*, *6*(8), 2563-2572. https://doi.org/10.1534/g3.116.031880

Patel, A., Lee, H. O., Jawerth, L., Maharana, S., Jahnel, M., Hein, M. Y., Stoynov, S., Mahamid, J., Saha, S., Franzmann, T. M., Pozniakovski, A., Poser, I., Maghelli, N., Royer, L. A., Weigert, M., Myers, E. W., Grill, S., Drechsel, D., Hyman, A. A., & Alberti, S. (2015). A Liquid-to-Solid Phase Transition of the ALS Protein FUS Accelerated by Disease Mutation. *Cell*, *162*(5), 1066-1077. https://doi.org/10.1016/j.cell.2015.07.047

Pek, J. W., Patil, V. S., & Kai, T. (2012). piRNA pathway and the potential processing site, the nuage, in the Drosophila germline. *Dev Growth Differ*, *54*(1), 66-77. https://doi.org/10.1111/j.1440-169x.2011.01316.x

Pham, J. W., Pellino, J. L., Lee, Y. S., Carthew, R. W., & Sontheimer, E. J. (2004). A Dicer-2-Dependent 80S Complex Cleaves Targeted mRNAs during RNAi in Drosophila. *Cell*, *117*, 83-94.

Polymenidou, M. (2018). The RNA face of phase separation. *Cell Biology*, *360*(6391), 859-860. https://doi.org/10.1126/science.aat8028

Polymenidou, M., Lagier-Tourenne, C., Hutt, K. R., Bennett, C. F., Cleveland, D. W., & Yeo, G. W. (2012). Misregulated RNA processing in amyotrophic lateral sclerosis. *Brain Res*, *1462*, 3-15. https://doi.org/10.1016/j.brainres.2012.02.059

Pratt, A. J., & MacRae, I. J. (2009). The RNA-induced silencing complex: a versatile gene-silencing machine. *J Biol Chem*, *284*(27), 17897-17901. https://doi.org/10.1074/jbc.R900012200

Rabouille, C., & Alberti, S. (2017). Cell adaptation upon stress: the emerging role of membrane-less compartments. *Curr Opin Cell Biol*, *47*, 34-42. https://doi.org/10.1016/j.ceb.2017.02.006

Rechavi, O., Houri-Ze'evi, L., Anava, S., Goh, W. S. S., Kerk, S. Y., Hannon, G. J., & Hobert, O. (2014). Starvation-induced transgenerational inheritance of small RNAs in C. elegans. *Cell*, *158*(2), 277-287. https://doi.org/10.1016/j.cell.2014.06.020

Ruff, K. M., Roberts, S., Chilkoti, A., & Pappu, R. V. (2018). Advances in Understanding Stimulus-Responsive Phase Behavior of Intrinsically Disordered Protein Polymers. *J Mol Biol*, *430*(23), 4619-4635. https://doi.org/10.1016/j.jmb.2018.06.031

Schirle, N. T., & MacRae, I. J. (2012). The crystal structure of human Argonaute2. *Science*, *336*(6084), 1037-1040. https://doi.org/10.1126/science.1221551

Schmidt, T., Knick, P., Lilie, H., Friedrich, S., Golbik, R. P., & Behrens, S. E. (2016). Coordinated Action of Two Double-Stranded RNA Binding Motifs and an RGG Motif Enables Nuclear Factor 90 To Flexibly Target Different RNA Substrates. *Biochemistry*, *55*(6), 948-959. https://doi.org/10.1021/acs.biochem.5b01072

Schuster, B. S., Regy, R. M., Dolan, E. M., Kanchi Ranganath, A., Jovic, N., Khare, S. D., Shi, Z., & Mittal, J. (2021). Biomolecular Condensates: Sequence Determinants of Phase Separation, Microstructural Organization, Enzymatic Activity, and Material Properties. *J Phys Chem B*, *125*(14), 3441-3451. https://doi.org/10.1021/acs.jpcb.0c11606

Schwarz, D. S., Hutvagner, G., Haley, B., & Zamore, P. D. (2002). Evidence that siRNAs Function as Guides, Not Primers, in the Drosophila and Human RNAi Pathways. *Mol Cell*, *10*, 537-548.

Shin, Y., & Brangwynne, C. P. (2017). Liquid phase condensation in cell physiology and disease. *Science*, *357*(6357). https://doi.org/10.1126/science.aaf4382

Soleimani, S., Valizadeh Arshad, Z., Moradi, S., Ahmadi, A., Davarpanah, S. J., & Azimzadeh Jamalkandi, S. (2020). Small regulatory noncoding RNAs in Drosophila melanogaster: biogenesis and biological functions. *Brief Funct Genomics*, *19*(4), 309-323. https://doi.org/10.1093/bfgp/elaa005

Spracklin, G., Fields, B., Wan, G., Becker, D., Wallig, A., Shukla, A., & Kennedy, S. (2017). The RNAi Inheritance Machinery of Caenorhabditis elegans. *Genetics*, *206*(3), 1403-1416. https://doi.org/10.1534/genetics.116.198812

Su, S., Wang, J., Deng, T., Yuan, X., He, J., Liu, N., Li, X., Huang, Y., Wang, H. W., & Ma, J. (2022). Structural insights into dsRNA processing by Drosophila Dicer-2-Loqs-PD. *Nature*, *607*(7918), 399-406. https://doi.org/10.1038/s41586-022-04911-x

Su, X., Ditlev, J. A., Hui, E., YXing, W., Banjade, S., Okrut, J., King, D. S., Taunton, J., Rosen, M. K., & Vale, R. D. (2016). Phase separation of signaling molecules promotes T cell receptor signal transduction. *Science*, *352*(6285), 595-599.

Svobodova, E., Kubikova, J., & Svoboda, P. (2016). Production of small RNAs by mammalian Dicer. *Pflugers Arch*, *468*(6), 1089-1102. https://doi.org/10.1007/s00424-016-1817-6

Tabara, H., Yigit, E., Siomi, H., & Mello, C. C. (2002). The dsRNA Binding Protein RDE-4 Interacts with RDE-1, DCR-1, and a DExH-Box Helicase to Direct RNAi in C.elegans. *Cell*, *109*(7), 861-871.

Tants, J. N., Fesser, S., Kern, T., Stehle, R., Geerlof, A., Wunderlich, C., Juen, M., Hartlmuller, C., Bottcher, R., Kunzelmann, S., Lange, O., Kreutz, C., Forstemann, K., & Sattler, M. (2017). Molecular basis for asymmetry sensing of siRNAs by the Drosophila Loqs-PD/Dcr-2 complex in RNA interference. *Nucleic Acids Res*, *45*(21), 12536-12550. https://doi.org/10.1093/nar/gkx886

Taylor, N. O., Wei, M. T., Stone, H. A., & Brangwynne, C. P. (2019). Quantifying Dynamics in Phase-Separated Condensates Using Fluorescence Recovery after Photobleaching. *Biophys J*, *117*(7), 1285-1300. https://doi.org/10.1016/j.bpj.2019.08.030

Thandapani, P., O'Connor, T. R., Bailey, T. L., & Richard, S. (2013). Defining the RGG/RG motif. *Mol Cell*, *50*(5), 613-623. https://doi.org/10.1016/j.molcel.2013.05.021

Tomari, Y., Matranga, C., Haley, B., Martinez, N., & Zamore, P. D. (2004). A Protein Sensor for siRNA Asymmetry. *Science*, *306*.

Wang, J., Choi, J. M., Holehouse, A. S., Lee, H. O., Zhang, X., Jahnel, M., Maharana, S., Lemaitre, R., Pozniakovsky, A., Drechsel, D., Poser, I., Pappu, R. V., Alberti, S., & Hyman, A. A.

(2018). A Molecular Grammar Governing the Driving Forces for Phase Separation of Prion-like RNA Binding Proteins. *Cell*, *174*(3), 688-699 e616. https://doi.org/10.1016/j.cell.2018.06.006

Wang, X., Vukovic, L., Koh, H. R., Schulten, K., & Myong, S. (2015). Dynamic profiling of double-stranded RNA binding proteins. *Nucleic Acids Res*, *43*(15), 7566-7576. https://doi.org/10.1093/nar/gkv726

Wang, Y., Lomakin, A., Kanai, S., Alex, R., & Benedek, G. B. (2017). Liquid-Liquid Phase Separation in Oligomeric Peptide Solutions. *Langmuir*, *33*(31), 7715-7721. https://doi.org/10.1021/acs.langmuir.7b01693

Weiberg, A., Bellinger, M., & Jin, H. (2015). Conversations between kingdoms: small RNAs. *Curr Opin Biotechnol*, *32*, 207-215. https://doi.org/10.1016/j.copbio.2014.12.025

Wheeler, R. J., & Hyman, A. A. (2018). Controlling compartmentalization by non-membrane-bound organelles. *Philos Trans R Soc Lond B Biol Sci*, *373*(1747). https://doi.org/10.1098/rstb.2017.0193

Wu, H. (2013). Higher-order assemblies in a new paradigm of signal transduction. *Cell*, *153*(2), 287-292. https://doi.org/10.1016/j.cell.2013.03.013

Yamaguchi, S., Naganuma, M., Nishizawa, T., Kusakizako, T., Tomari, Y., Nishimasu, H., & Nureki, O. (2022). Structure of the Dicer-2-R2D2 heterodimer bound to a small RNA duplex. *Nature*, *607*(7918), 393-398. https://doi.org/10.1038/s41586-022-04790-2

Yi, R., Qin, Y., Macara, I. G., & Cullen, B. R. (2003). Exportin-5 mediates the nuclear export of pre-microRNAs and short hairpin RNAs. *Genes Dev*, *17*(24), 3011-3016. https://doi.org/10.1101/gad.1158803

Yigit, E., Batista, P. J., Bei, Y., Pang, K. M., Chen, C. C., Tolia, N. H., Joshua-Tor, L., Mitani, S., Simard, M. J., & Mello, C. C. (2006). Analysis of the C. elegans Argonaute family reveals that distinct Argonautes act sequentially during RNAi. *Cell*, *127*(4), 747-757. https://doi.org/10.1016/j.cell.2006.09.033

Zeng, Y., & Cullen, B. R. (2004). Structural requirements for pre-microRNA binding and nuclear export by Exportin 5. *Nucleic Acids Res*, *32*(16), 4776-4785. https://doi.org/10.1093/nar/gkh824

Zhou, R., Czech, B., Brennecke, J., Sachidanandam, R., Wohlschlegel, J. A., Perrimon, N., & Hannon, G. J. (2009). Processing of Drosophila endo-siRNAs depends on a specific Loquacious isoform. *RNA*, *15*(10), 1886-1895. https://doi.org/10.1261/rna.1611309

6 Acknowledgements

First of all, I would like to express my gratitude to my supervisor Prof. Dr. Klaus Förstemann for the support and motivation that guided me through the project and to the completion of my thesis.

I would like to thank the members of my TAC Prof. Dr. Johannes Stigler and Hyun Seo Kang Ph.D. for their helpful advice during our meetings and our collaborators from the Sattler-lab at TU Munich. In addition, I would like to thank the technical and support staff of the Gene Center Munich and in particular Dr. Christophe Jung (Imaging Facility).

Special thanks go to all of the current and former lab members, especially to Romy Böttcher, Petar Duric and Volker Nitschko. Thank you very much for the time spent together – inside and outside the lab – and for your ongoing encouragement and help.

Last but not least, many thanks to my family and friends.